CMS Physics Analysis Summary

Contact: cms-pag-conveners-higgs@cern.ch 2011/08/22

Search for standard model Higgs boson in pp collisions at $\sqrt{s} = 7$ TeV and integrated luminosity up to 1.7 fb^{-1}

The CMS Collaboration

Abstract

The overall combination is presented of eight standard model (SM) Higgs boson searches performed by the CMS Collaboration using the following Higgs boson decay signatures: $H \to \gamma\gamma$, $H \to \tau\tau$, $H \to bb$, $H \to WW \to 2\ell 2\nu$, $H \to ZZ \to 4\ell$, $H \to ZZ \to 2\ell 2\tau$, $H \to ZZ \to 2\ell 2\nu$, and $H \to ZZ \to 2\ell 2q$. Depending on the analysis, the amount of data used corresponds to 1.1-1.7 fb^{-1} of integrated luminosity. The SM Higgs boson is excluded at 95% C.L. in three mass ranges 145-216, 226-288, and 310-400 GeV/c^2. The expected exclusion in the absence of a signal is 130-440 GeV/c^2. The largest excursion of the observed data from the expected has a probability of 0.4 after taking into account the look-elsewhere effect. At 90% C.L., we exclude the SM Higgs boson in the continuous mass range from 144-440 GeV/c^2. The reported limits were obtained using the modified frequentist construction known as the CL$_s$ method.

1 Introduction

The discovery of the mechanism for electroweak symmetry breaking is one of the key parts of the Large Hadron Collider (LHC) physics program. In the standard model (SM), this can be achieved by invoking what has become known as the Higgs mechanism, leading to the prediction of the Higgs boson [1–6]. The Higgs boson mass is essentially the only unknown in the model, all other parameters being reasonably well constrained by existing measurements. To date, the experimental searches for this elusive particle have yielded negative results and limits on its mass have been placed by experiments at LEP, $m_H > 114.4$ GeV/c^2 [7], and the Tevatron, $m_H \notin [100, 109]$ and $m_H \notin [156, 177]$ GeV/c^2 [8]. Fits of the electroweak precision measurements, not taking into account the direct search results, constrain indirectly the SM Higgs boson mass to be relatively light, $m_H < 158$ GeV/c^2 [9]. All limits quoted in this note are at 95% C.L. unless explicitly stated otherwise.

The CMS Experiment [10] was designed to be able to detect a Higgs boson with a mass ranging from the LEP lower mass bound up to roughly 1 TeV/c^2. Depending on the Higgs boson mass various production mechanisms and decay channels are possible and are actively being pursued. In this note, we report the overall combination of the search results obtained in the following eight analyses, grouped by the Higgs decay modes: $H \to \gamma\gamma$ [11], $H \to \tau\tau$ [12], $H \to bb$ [13], $H \to WW \to 2\ell 2\nu$ [14], $H \to ZZ \to 4\ell$ [15], $H \to ZZ \to 2\ell 2\tau$ [16], $H \to ZZ \to 2\ell 2\nu$ [17], and $H \to ZZ \to 2\ell 2q$ [18]. Each of these analyses has a number of sub-channels that add up to a total of 43 independent signatures entering the overall combination. The choice of the Higgs boson mass points used in the analyses and the overall combination is driven by either instrumental $\gamma\gamma/4\ell$ mass resolutions (for $m_H < 250$ GeV/c^2) or by the expected standard model Higgs boson width at higher masses.

The cross sections, together with their uncertainties, for each Higgs boson production mechanism and decay branching ratios are taken from the CERN Yellow Report prepared by the LHC Higgs Cross Section Group [19]. The gg-fusion cross section is calculated at NNLO$_{QCD}$ + NNLL$_{QCD}$ + NLO$_{EWK}$ precision, the vector boson fusion (VBF) and the associated WH and ZH cross sections—at NNLO$_{QCD}$ + NLO$_{EWK}$ precision, and $t\bar{t}H$ at NLO$_{QCD}$ precision. The errors on the branching ratios are generally very small and have been neglected in most of the analyses presented in this note. Uncertainties on the Higgs boson mass lineshape and its impact on the cross section for a Higgs boson with very large mass ($m_H > 400$ GeV/c^2) are not yet included.

In Section 2, we briefly outline the overall statistical model used in this work. In Section 3, we give a brief overview of each analysis entering the overall combination. And finally, in Section 4, we present our main results.

2 Statistical Analysis

A statistical combination of results of multiple searches furthers the overall experimental sensitivity to the presence or absence of new physics in comparison to what otherwise could be inferred from each analysis on its own. The challenge of such an undertaking is to put all analyses in the same framework and understand the role of different systematic errors, including their inter-channel correlations. In this section, we describe our choices for modeling systematic uncertainties in general and which ones we would treat as correlated, in particular. We also give a brief summary of the statistical methods and software tools we use for quantifying the search results presented in this note.

Notations

In the following, the expected SM Higgs event yields are generically denoted as s, and backgrounds as b. These stand for event counts in one or multiple bins or for probability density functions, whichever is used in an analysis. Predictions for both signal and background yields, prior to the likelihood fit of the data entering the statistical analysis, are subject to multiple uncertainties that are handled by introducing nuisance parameters θ, so that signal and background expectations become functions of the nuisance parameters: $s(\theta)$ and $b(\theta)$. The events actually observed are denoted as an *observation*. It has become customary to represent the negative SM Higgs search results as limits on a common *signal strength modifier* μ that is defined as the ratio of the true cross section to the SM predicted one.

Modeling of systematic uncertainties

We follow the procedure and definitions for the terms below from Ref. [20]. All systematic errors are treated as either 100% correlated (positively or negatively) or independent. Partially correlated errors are broken down further to independent sources or declared to be correlated/uncorrelated, whichever is judged to be a better approximation or more conservative. Each independent source of uncertainty is associated to a nuisance parameter θ. Correlated uncertainties driven by the same nuisance parameter need not have the same scale.

For the calculations described below, we need to model the sources of uncertainty. This is done with the help of priors in Bayesian calculations, and measurement probability distribution functions (*pdf*s) in frequentist ones. Below are the types of priors $\rho(\theta \mid \tilde{\theta})$ used in combination presented in this note. Their frequentist counterpart *pdf*s are introduced in the next sub-section.

- Nuisance parameters, unconstrained by any a priori considerations and/or measurements, are assigned *flat priors*.
- Nuisance parameters that can take both positive and negative values are generally described by *Gaussian distributions* with some mean value $\tilde{\theta}$ and width parameter σ.
- Systematic uncertainties on observables that can take only positive values (cross sections, integrated luminosity, selection efficiencies, etc.) are generally described by *log-normal distributions*. They are characterized by the parameter κ, a factor by which the true value of an observable can be larger or smaller than its default. Technically, log-normal errors are modeled by writing an observable A in the following form $A = A_0 \cdot \kappa^{\theta}$, where θ is a nuisance parameter with the normal pdf. In other words, log-normal errors can be and are handled via normal pdf constraints.
- Uncertainties of statistical nature (e.g., statistical error associated with a number of events simulated in MC or a number of observed events in a control region) are described with *gamma distributions*. The width of the gamma distribution is determined by the number of simulated or observed events.

Modified frequentist limits (CL_s)

As the prime method for reporting limits in this note, we use the modified frequentist construction (often referred to as CL_s) [21, 22]. To fully define the method, one needs to make a choice of the test statistic and how one would treat nuisance parameters in the construction of the test statistic and in generating pseudo-data. In this note, we follow the prescription prepared by the LHC Higgs Combination Group [20]. Below is a brief outline of the procedure.

The first step is to re-interpret systematic error pdfs $\rho(\theta|\tilde{\theta})$ as posteriors arising from some

"real" or "imaginary" measurements $\tilde{\theta}$, as given by the Bayes' theorem:

$$\rho(\theta|\tilde{\theta}) \;\sim\; p(\tilde{\theta}\,|\,\theta)\cdot\pi_\theta(\theta), \tag{1}$$

where $\pi_\theta(\theta)$ functions are hyper-priors for those "measurements". These hyper-priors are chosen to be uniform (flat) distributions. With this choice, $\rho(\theta\,|\,\tilde{\theta})$ will be a gamma distribution if $p(\tilde{\theta}\,|\,\theta)$ is Poisson, and normal if $p(\tilde{\theta}\,|\,\theta)$ is normal. This approach allows sampling distributions for the test statistic to be constructed in a purely frequentist manner.

The likelihood $\mathcal{L}(data\,|\,\mu,\theta)$ to be used in constructing the test statistic is defined as follows:

$$\mathcal{L}(data\,|\,\mu,\theta) = \text{Poisson}\,(\,data\,|\,\mu\cdot s(\theta)+b(\theta)\,)\cdot p(\tilde{\theta}|\theta)\,, \tag{2}$$

where Poisson $(\,data\,|\,\mu s(\theta)+b(\theta)\,)$ is the Poisson probability to observe *data*, assuming signal and background models, $s(\theta)$ and $b(\theta)$, that depend on some nuisance parameters θ.

The test statistic is then defined as the profile likelihood ratio:

$$q_\mu \;=\; -2\ln\frac{\mathcal{L}(\text{data}|\mu,\hat{\theta}_\mu)}{\mathcal{L}(\text{data}|\hat{\mu},\hat{\theta})}, \quad \text{with a constraint } 0\le\hat{\mu}\le\mu \tag{3}$$

where "data" can be the actual *observation* or pseudo-data. Both the denominator and numerator are maximized. In the numerator, μ remains fixed and only the nuisance parameters θ are allowed to float. Their values at which $\mathcal{L}$ reaches the maximum are denoted as $\hat{\theta}_\mu$. In the denominator, both μ and θ are allowed to float in the fit, and $\hat{\mu}$ and $\hat{\theta}$ are parameters at which $\mathcal{L}$ reaches its global maximum. The lower constraint on $\hat{\mu}$ ($0\le\hat{\mu}$) is imposed by hand as the signal rate cannot be negative. The upper constraint ($\hat{\mu}\le\mu$) forces the limit to be one-sided. For observations preferring the best-fit values of $\hat{\mu}>\mu$, the test statistic collapses to zero. The value of the test statistic for the actual observation will be denoted as q_μ^{obs}.

Next, we find the values of nuisance parameters $\hat{\theta}_0^{obs}$ and $\hat{\theta}_\mu^{obs}$ best describing the experimentally *observed* data (i.e. maximizing $\mathcal{L}$), for the *background-only* and *signal+background* hypotheses, respectively. Using these best-fit values of nuisance parameters, we generate toy Monte Carlo pseudo-data to construct the test statistic *pdf*s assuming a signal with strength μ and for the *background-only* hypothesis ($\mu=0$). The "measurements" $\tilde{\theta}$ are also randomized in each pseudo-data, using the *pdf*s $p(\tilde{\theta}|\theta)$ from Eq. (1). Note, that for the purposes of pseudo-data generation, the nuisance parameters are fixed to their data-driven best-fit values $\hat{\theta}_\mu^{\text{obs}}$ or $\hat{\theta}_0^{\text{obs}}$, but are allowed to float in fits needed to evaluate the test statistic. An example of two such sampling *pdf*s is given in Fig. 1 (left). These sampling distributions are obtained for the actual combination for a Higgs boson mass $m_H=250\ \text{GeV}/c^2$.

Having constructed two such *pdf*s, we find two p-values to be associated with the actual observation for the *signal+background* and *background-only* hypotheses, p_μ and p_0:

$$P\left(\,q_\mu\ge q_\mu^{obs}\,|\,\mu s(\hat{\theta}_\mu^{obs})+b(\hat{\theta}_\mu^{obs})\right)\,, \tag{4}$$

$$P\left(\,q_\mu\ge q_\mu^{obs}\,|\,b(\hat{\theta}_0^{obs})\right)\,, \tag{5}$$

and calculate $\text{CL}_\text{s}(\mu)$ as a ratio of these two p-values,

$$CL_s(\mu)=\frac{P\left(\,q_\mu\ge q_\mu^{obs}\,|\,\mu s(\hat{\theta}_\mu^{obs})+b(\hat{\theta}_\mu^{obs})\right)}{P\left(\,q_\mu\ge q_\mu^{obs}\,|\,b(\hat{\theta}_0^{obs})\right)}\,. \tag{6}$$

If $CL_s \leq \alpha$ for $\mu = 1$, we say that the SM Higgs boson is excluded at the $(1-\alpha)$ Confidence Level (C.L.). It is known that the CL_s method gives conservative limits, i.e. the actual confidence level is higher than $(1-\alpha)$.

To quote the 95% Confidence Level upper limit on μ, to be further denoted as $\mu^{95\%CL}$, we adjust μ until we reach $CL_s = 0.05$.

The detailed discussion of differences between the three flavors of CL_s, LEP-type [23] , Tevatron-type [24–26], and the one defined by the LHC Higgs Combination group (and briefly outlined above), can be found elsewhere [20]. In brief, the main differences are:

- Both LEP and Tevatron used the test statistic with fixed $\mu = 0$ in the denominator (cf. Eq. 3), which does not guarantee the desired asymptotic behavior allowing the approximate evaluation of p-values from the value of the observed test statistic itself, without having to generate large amounts of pseudo-data.
- LEP did not profile systematic errors in the test statistic, which does not allow one to take advantage of the constraints arising from the data used in the statistical analysis. Tevatron does profile systematic errors as we do.
- Both LEP and Tevatron used a Bayesian-frequentist approach to handling systematic uncertainties in generating sampling distributions, while we use a pure frequentist

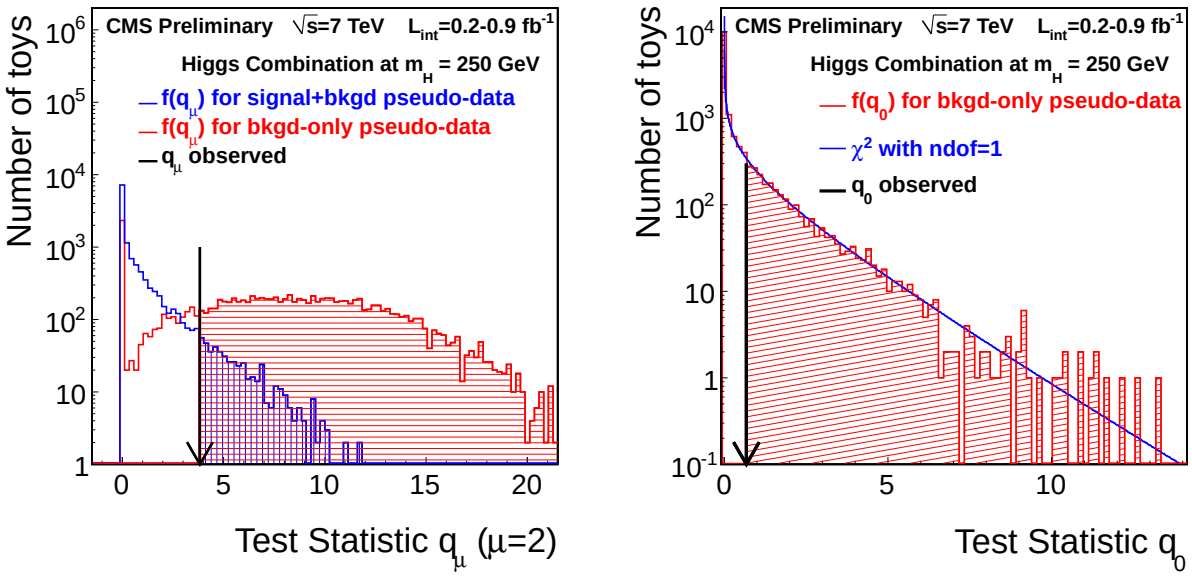

Figure 1: (Left) Frequentist tests statistic q_μ for distributions of ensembles of pseudo-data generated for *background-only* and *signal+background* hypotheses. The signal strength assumed in this example is $\mu = 2$. The observed value of the test statistic q_μ^{obs} is indicated by the arrow. Probabilities to find an observation above this value for the *background-only* and *signal+background* hypotheses are $P\left(q_\mu \geq q_\mu^{obs} \mid b(\hat{\theta}_0^{obs})\right) = 0.868 \pm 0.005$ and $P\left(q_\mu \geq q_\mu^{obs} \mid \mu s(\hat{\theta}_\mu^{obs}) + b(\hat{\theta}_\mu^{obs})\right) = 0.040 \pm 0.002$, respectively, resulting in $CL_s = 0.046 \pm 0.002$. (Right) Frequentist tests statistic q_0 for distributions for an ensemble of pseudo-data generated for the *background-only* hypotheses. The curve is the asymptotic χ^2 distribution for one degree of freedom. The observed value of the test statistic q_0^{obs} is indicated by the arrow. The true p-value of such an observation, i.e. probability $P(q_0 \geq q_0^{obs})$, as obtained form the sampling distribution is 0.180 ± 0.004, while the approximate $\tilde{p}$-value, as given by Eq. (9), is 0.218.

approach.

Numerically, results derived from the Tevatron-type and LHC-type CL_s definitions are found to be very similar.

Quantifying significance of an excess of events

To quantify an excess of events, we use the test statistic q_0, defined as follows:

$$q_0 \;=\; -2\ln\frac{\mathcal{L}(\text{data}|0,\hat{\hat{\theta}}_0)}{\mathcal{L}(\text{data}|\hat{\mu},\hat{\theta})} \quad \text{and } \hat{\mu} \geq 0. \tag{7}$$

This test statistic is known to have a half χ^2 distribution for one degree of freedom, which allows us to evaluate significances (Z) and p-values (p_0) from the following asymptotic formula, derived from the asymptotic properties of the test statistic based on the profile likelihood ratio [27]:

$$Z = \sqrt{q_0^{\text{obs}}}, \tag{8}$$

$$p_0 \;=\; P(q_0 \geq q_0^{\text{obs}}) \;=\; \int_Z^\infty \frac{e^{-x^2/2}}{\sqrt{2\pi}}\,dx \;=\; \frac{1}{2}\left[1-\text{erf}\left(Z/\sqrt{2}\right)\right], \tag{9}$$

where q_0^{obs} is the observed test statistic calculated for $\mu = 0$ and with only one constraint $0 \leq \hat{\mu}$, which ensures that data deficits are not counted on an equal footing with data excesses. The approximation has been tested and works well for the range of expected background and signal yields. Figure 1 (right) gives an example of the distribution of the test statistic q_0. One can see that the test statistic sampling distribution agrees well with the approximation shown as a curve. This sampling distribution is obtained for the actual combination for a Higgs boson mass $m_H = 250\ \text{GeV}/c^2$. To quote significance, we choose a "one-sided Gaussian" convention for associating p-value and significance Z.

Due to a significant Look-Elsewhere Effect (LEE) inevitable in a search for a signal in a very broad mass range, the observed minimum *local* p-value p_0^{min} (and the corresponding maximum significance Z_{max}) may be misleading. Following the prescription outlined in Ref. [20], the global probability p_0^{global} to observe p_0^{min}, or lower, can be *estimated* by counting the number of times the observed $q_0(m_H)$ crosses over (in one direction) some low threshold line. To increase the statistical precision of the estimate, we choose the threshold at lowest possible level $q_0(m_H) = 0$, or equivalently $\hat{\mu} = 0$ or $p_0 = 0.5$. If one counts the number of such crossings N_0 at this lowest level, then, the *estimated* global probability becomes [28]:

$$p_0^{\text{global}} \sim p_0^{\text{min}} + N_0\, e^{-\frac{1}{2}Z_{\text{max}}^2}. \tag{10}$$

Statistical analysis tools

All results quoted in this paper are validated by using two independent sets of software tools, RooStats [29] and L&S [30]. Both have been made to run off the same input information provided by the individual analyses for each channel. We find precise agreement of test statistics obtained using these two very different software implementations. In addition, many cross checks were done between the independent combination tools of CMS and ATLAS in terms of reproducibility for a large set of test scenarios [20]. The computational precision on all results reported in this note is at the level of O(1%) of the quoted numbers, unless stated otherwise.

3 Search channels used in the combination

The combination presented in this note is based on eight major channels classified by the final Higgs decay chain signature as shown in Table 1. The mass search regions are specific to each analysis. The analyzed integrated luminosity varies from channel to channel in the range from 1.1-1.7 fb^{-1}.

From Table 1, one can also see that different analysis strategies are employed in different searches. They include three basic types: cut-and-count analyses, analyses of binned distributions, and unbinned analyses tracking individual events and using parametric models of signal and background shapes.

Each of the major analyses is a combination in itself with 2 to 8 independent sub-channels. In the overall combination there are 27 independent sub-channels at low mass Higgs boson searches ($m_H < 135\,\mathrm{GeV}/c^2$) and 24 sub-channels in the high mass region ($m_H > 250\,\mathrm{GeV}/c^2$).

The last column in Table 1 shows the number of nuisance parameters (systematic uncertainties) in each analysis. The total number of independent nuisance parameters in the current combination is 267, of which 241 are used in the combination in the low mass range and 146 in the high mass range. There are 25 correlated sources of uncertainties appearing in more than one major search. The remaining ones are specific to individual analyses [1].

Table 2 shows the full list of uncertainties correlated across more than one major analysis. The top block in the table is a subset of the list prepared by the LHC Higgs Combination Group [20]. The bottom block are correlated errors that are correlated within CMS only. Quantities affected by the uncertainties listed in Table 2 are all positive definite and, hence, modeled as log-normals.

In the following subsections, we give a brief description of search strategies for the eight channels used in this combination. Detailed information can be found in references provided within each sub-section.

Table 1: Summary information on the analyses included in the combination. The first number in the last column gives the number of nuisance parameters correlated across two or more analyses. The second number refers to the number of nuisance parameters specific to one analysis only.

channel	mass range (GeV/c^2)	luminosity (fb^{-1})	number of sub-channels	type of analysis	number of nuisances
$H \to \gamma\gamma$	110-150	1.7	8	mass shape (unbinned)	3+40=43
$H \to \tau\tau$	110-140	1.1	6	mass shape (binned)	10+25=35
$H \to bb$	110-135	1.1	5	cut&count	10+59 = 69
$H \to WW \to 2\ell 2\nu$	110-600	1.5	5	cut&count	15 +79 =94
$H \to ZZ \to 4\ell$	110-600	1.7	3	mass shape (unbinned)	14+20=34
$H \to ZZ \to 2\ell 2\tau$	180-600	1.1	8	mass shape (unbinned)	13+10=23
$H \to ZZ \to 2\ell 2\nu$	250-600	1.6	2	cut&count	14+4=18
$H \to ZZ \to 2\ell 2q$	226-600	1.6	6	mass shape (unbinned)	12+15=27
TOTAL (8)	110-600	1.1-1.7	27 for low m_H 24 for high m_H		241 for low m_H 146 for high m_H

[1] The majority of them are actually also correlated between different sub-channels within an analysis.

Table 2: Correlated systematic uncertainties in the analyses contributing to the combination. Uncertainties associated with the photon reconstruction are not in the table as they appear only in one analysis.

group	nuisance	comments
cross section (pdf)	gg	$gg \to H$, $t\bar{t}H$, VQQ, $t\bar{t}$, tW, tb (s-channel), $gg \to VV$
	qqbar	VBF H, VH, V, VV, $\gamma\gamma$
cross section (QCD scales)	ggH	total inclusive $gg \to H$
	ggH1in	inclusive $gg/qg \to H+ \geq 1$ jets
	ggH2in	inclusive $gg/qg \to H+ \geq 2$ jets
	qqH	VBF H
	VH	associate VH
	ttH	$t\bar{t}H$
	VV	WW, WZ, and ZZ up to NLO
	ggVV	$gg \to WW$ and $gg \to ZZ$
Higgs BR	ZZ	Branching ratio BR($H \to ZZ$)
phenomenology	UE & PS	modeling of underlying event (UE) and parton showering (PS)
luminosity	lumi	uncertainties in integrated luminosity
efficiencies	muon	prompt muon efficiency (includes reconstruction, isolation)
	electron	prompt electron efficiency (includes reconstruction, isolation)
	tau	reconstruction efficiency of prompt hadronicly decaying tau
	b-tag	b-tag efficiency for b-jets (anti-correlated with b-jet veto)
p_T scales	muon	prompt muon p_T-scale
	electron	prompt electron p_T-scale
	tau	p_T scale for prompt hadronicly decaying tau
	jets	jet energy scale
p_T resolutions	electron	prompt electron p_T-resolution
fake rates	lepton	determination of fake lepton rates in data
trigger efficiencies	muon	prompt muon efficiency (includes trigger, reconstruction, isolation)
	electron	prompt electron efficiency (includes trigger, reconstruction, isolation)

3.1 $H \to \gamma\gamma$ channel [11]

In this channel, the signal of a standard model Higgs boson is a narrow peak in the diphoton invariant mass distribution ($m_{\gamma\gamma}$), dominated by experimental resolutions, on a large falling background spectrum.

Events are first selected by requiring a diphoton trigger to have fired. Photon candidates, isolated in the tracking detectors and calorimeters, are required to pass a set of tight identification and quality cuts, reducing the background contributions from events with fake photons. Photon candidates must have a pseudorapidity, within the acceptance of the detector: $|\eta| < 2.5$ and outside the transition region between the barrel and endcap detectors: $1.4442 < |\eta| < 1.566$. The two photon candidates with the highest transverse momenta, E_{T} are selected to form the Higgs candidate and are required to satisfy, $E_{\mathrm{T}}^{\mathrm{lead}} > 40$ GeV and $E_{\mathrm{T}}^{\mathrm{sub-lead}} > 30$ GeV for the leading and sub-leading candidate, respectively.

For the data set under consideration, about six interactions per beam crossing, on average, are expected. The choice of reconstructed primary vertex has an impact on the mass resolution and hence on the sensitivity of the analysis. The reconstructed primary vertices are ranked according to the kinematic properties of the relevant charged tracks and the diphoton Higgs candidate. Where there is evidence for a photon having undergone pair production, the associated charged tracks are used to further refine the vertex choice.

The data are split into eight categories based on the eight permutations of whether or not:

- the transverse momentum of the diphoton system $p_{\mathrm{T}}^{\mathrm{Higgs}} > 40\,\mathrm{GeV}/c$;
- both photon candidates are in the barrel detector;
- both photons pass a cut on a discriminant loosely describing the shower shape that will reject photons likely to have undergone a conversion.

Simulated signal events are produced using the next-to-leading-order (NLO) matrix-element generator POWHEG [31] interfaced to PYTHIA [32] for parton showering. Reweighting of the Higgs p_{T} spectrum is carried out using the NLO+NNLL distribution computed by the HqT program [33]. Smearing of the photon energies is applied to account for differences between data and simulation. These are derived from detailed studies of $Z \to e^+e^-$ events. The best category di-photons give a peak with FWHM$/m_H = 2.4\%$ (full width at half maximum), the worst category—FWHM$/m_H = 6.5\%$ The signal is modelled in the statistical analysis based on a parameterized fit to the smeared and reweighted simulated events, consisting of a sum of two or three Gaussian distributions.

The dominant source of background comes from events containing two real prompt photons or one prompt and a fake from a jet. The contribution from double fakes is estimated to be small. The background is modelled parametrically directly from unbinned fits to the data using a second order Bernstein [34] polynomial constrained to be positive definite. There is no Monte Carlo input to these fits. Figures 2 and 3 show the binned data, the result of the unbinned fit for the background model (under the null background-only hypothesis), and the parameterized signal distribution (at 5×SM) for a hypothesized Higgs mass $m_H = 120\,\mathrm{GeV}/c^2$.

Systematic uncertainties on the signal model affecting both the yield and the shape are considered. The largest sources of uncertainty on the event yield arise from the uncertainty on the integrated luminosity (4.5%).

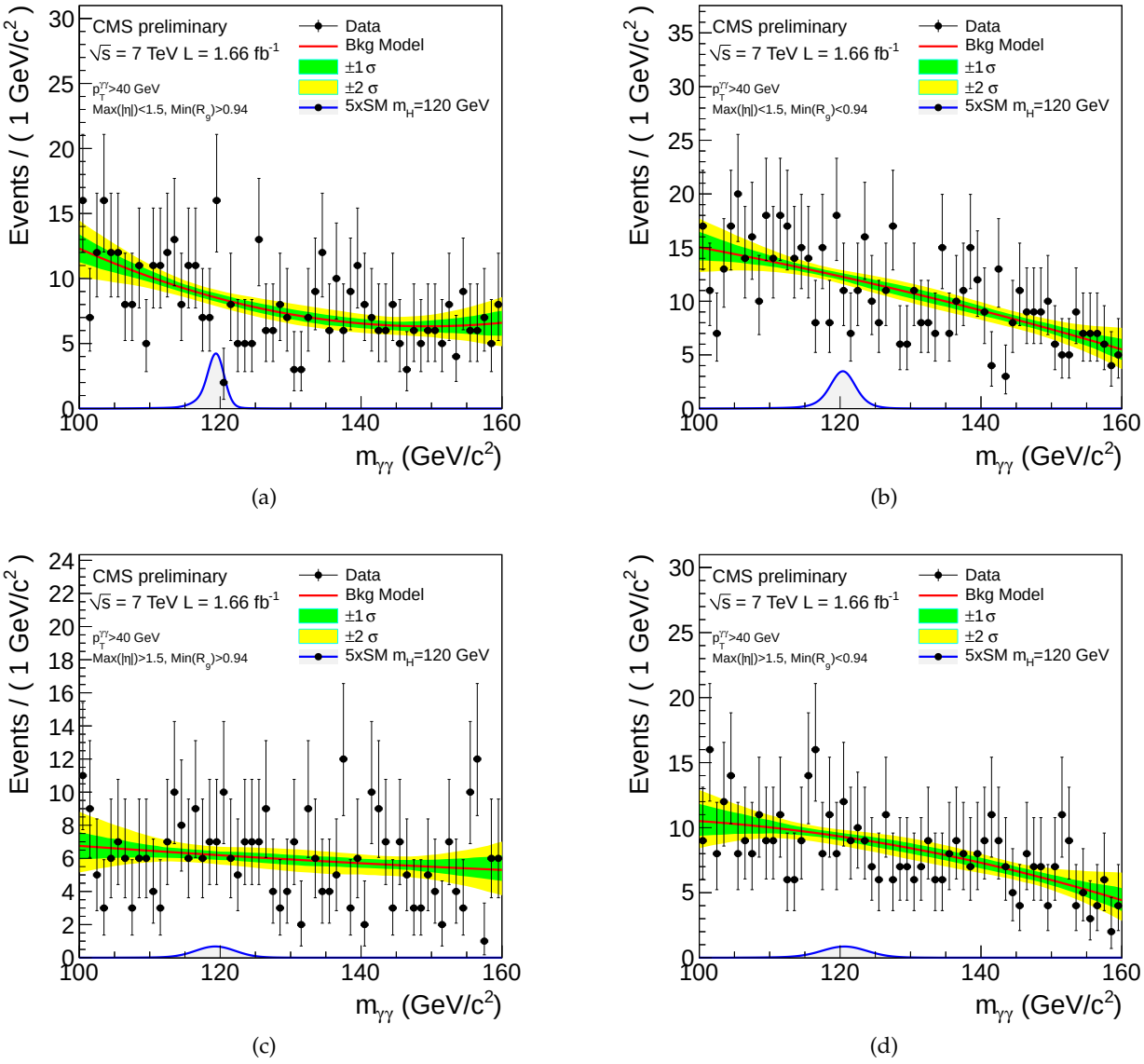

Figure 2: Binned $m_{\gamma\gamma}$ distributions for four event categories for di-photons with $p_T(\gamma\gamma) > 40$ GeV/c: (a) Both photons likely unconverted and in the barrel, (b) At least one photon likely to have undergone pair production, both are in the barrel, (c) Both photons likely unconverted and at least one photon in in the endcap, (d) At least one photon likely to have undergone pair production and at least one photon in the endcap. The Monte Carlo prediction and parameterized signal model for a Higgs boson mass $m_H = 120$ GeV/c^2 (5×SM) are also shown together with the result of the unbinned fit to the background model. The yellow/green bands indicate $\pm 1\sigma$ and $\pm 2\sigma$ errors on the background fit.

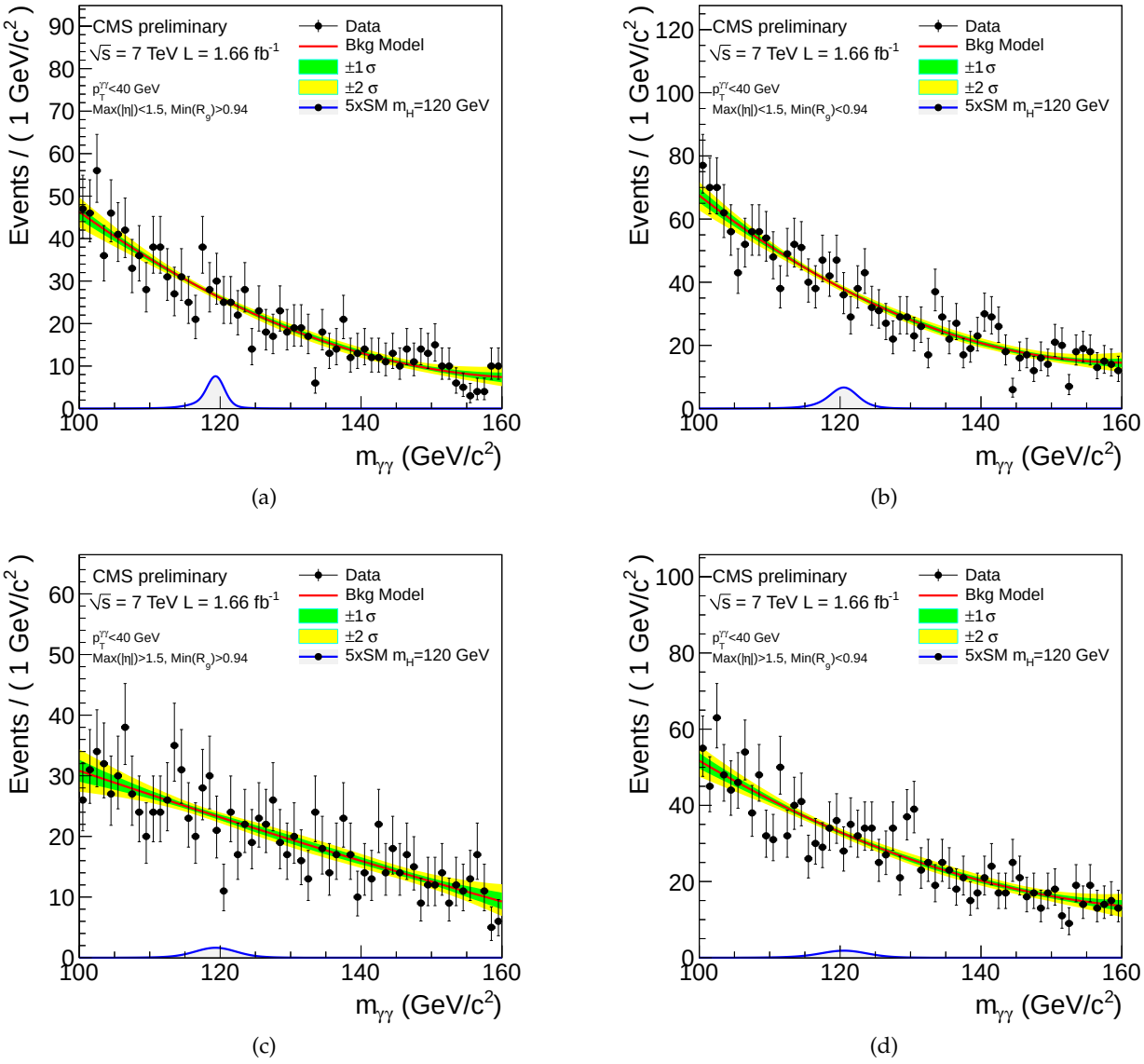

Figure 3: Binned $m_{\gamma\gamma}$ distributions for four event categories for di-photons with $p_T(\gamma\gamma) < 40$ GeV/c: (a) Both photons likely unconverted and in the barrel, (b) At least one photon likely to have undergone pair production, both are in the barrel, (c) Both photons likely unconverted and at least one photon in in the endcap, (d) At least one photon likely to have undergone pair production and at least one photon in the endcap. The Monte Carlo prediction and parameterized signal model for a Higgs boson mass $m_H = 120$ GeV/c^2 (5×SM) are also shown together with the result of the unbinned fit for the background model. The yellow/green bands indicate $\pm1\sigma$ and $\pm2\sigma$ errors on the background fit.

3.2 $H \to \tau\tau$ channel [12]

In this analysis, we search for an excess of events in the visible mass m_{vis} distributions of $e + \tau_{had}$, $\mu + \tau_{had}$ and $e + \mu$ final states [2] , each of which is further subdivided in two: with two VBF-like jets or not. Therefore, the search has in total 6 sub-channels. The visible mass is built from measured momenta of electrons, muons, and taus and does not attempt to recover the momentum carried away by neutrinos. The six mass distributions are binned and the entire shape is used in the statistical analysis.

Triggers requiring the presence of both a lepton and an isolated jet consistent with a τ decaying hadronically were adopted for the $e + \tau_{had}$, $\mu + \tau_{had}$ channels. The $e\mu$ events were collected using the di-lepton $e\mu$ trigger. For $e + \tau_{had}$, $\mu + \tau_{had}$ final states, we selected events with an isolated electron with $p_T > 20$ GeV/c or isolated muon with $p_T > 15$ GeV/c and $|\eta| < 2.1$, and an oppositely charged τ_{had} with $p_T > 20$ GeV/c and $|\eta| < 2.3$. For the $e\mu$ final state, we selected events with an isolated electron with $|\eta| < 2.5$ and an oppositely charged isolated muon with$|\eta| < 2.1$, both with $p_T > 15$ GeV/c. We rejected events with more than one e or μ. A toplogical cut based on the p_T vectors of the two leptons and the missing transverse energy E_T^{mis} is applied to exploit the fact that visible τ-decay products and neutrinos tend to be colinear.

Motivated by the prominent vector boson fusion component in the Higgs boson production, we split the sample of selected events into two sub-categories as follows:

- VBF: exactly 2 jets with $p_T > 30$ GeV/c, $m_{jj} > 350$ GeV/c^2, $|\Delta\eta_{jj}| > 3.5$, $\eta_1 \cdot \eta_2 < 0$.
- Non-VBF: ≤ 1 jet with $p_T > 30$ GeV/c, or exactly 2 jets that fail VBF requirements.

The final distribution to discriminate signal from background in each of the six sub-channels is the visible mass m_{vis}. The visible mass distributions for the VBF and non-VBF categories for the $e + \tau_{had}$, $\mu + \tau_{had}$ and $e + \mu$, after all the selection cuts, are shown in Figure 4. The visible mass resolution is about 20%.

The dominant irreducible background in this analysis is $Z \to \tau\tau$ production. The other three main backgrounds are Electroweak ($W(\ell\nu)$+jets, $Z(\ell\ell)$+jets), $t\bar{t}$, and QCD, in which one or both leptons are fakes.

The $Z \to \tau\tau$ shape is taken from Monte Carlo, while its normalization (total event yield) is constrained by $Z \to \ell\ell$ measurements and by the fit of the m_{vis} mass shape distribution. The $W(\ell\nu)$+jets and QCD backgrounds are dealt with by using two control samples: one with the topological cut inverted and another with same-sign di-lepton events. The normalizations for $Z(\ell\ell)$+jets (important for $e\tau$-channel), $t\bar{t}$, and di-bosons are taken from corresponding control samples without τ-leptons and scaling them by probabilities for electrons, muons, and jets to fake τ-leptons as measured directly from data.

The largest uncertainties on the signal yield include cross section (12% for ggH and 4% for VBF), integrated luminosity (4.5%), τ-identification (6%), and jet energy scale (5%). Other errors are O(1%). The largest background uncertainties for VBF categories come from statistical uncertainties for the number of events observed in control samples (up to 40%). For non-VBF selection, the largest background uncertainties are due to extrapolation factors from measurements done in control regions into the signal region: fake rates for electrons (8%) and jets (12%) for $Z(\ell\ell)$+jets background, opposite-sign to same-sign ratios for $W(\ell\nu)$+jets (6%) and QCD (6%), and $t\bar{t}$ extrapolation (11%). The mass shape uncertainties arising from variations in tau, electron, and muon energy scales—3%, 2%, and 1%, respectively—are also included.

[2] τ_{had} stands for τ-leptons decaying hadronically

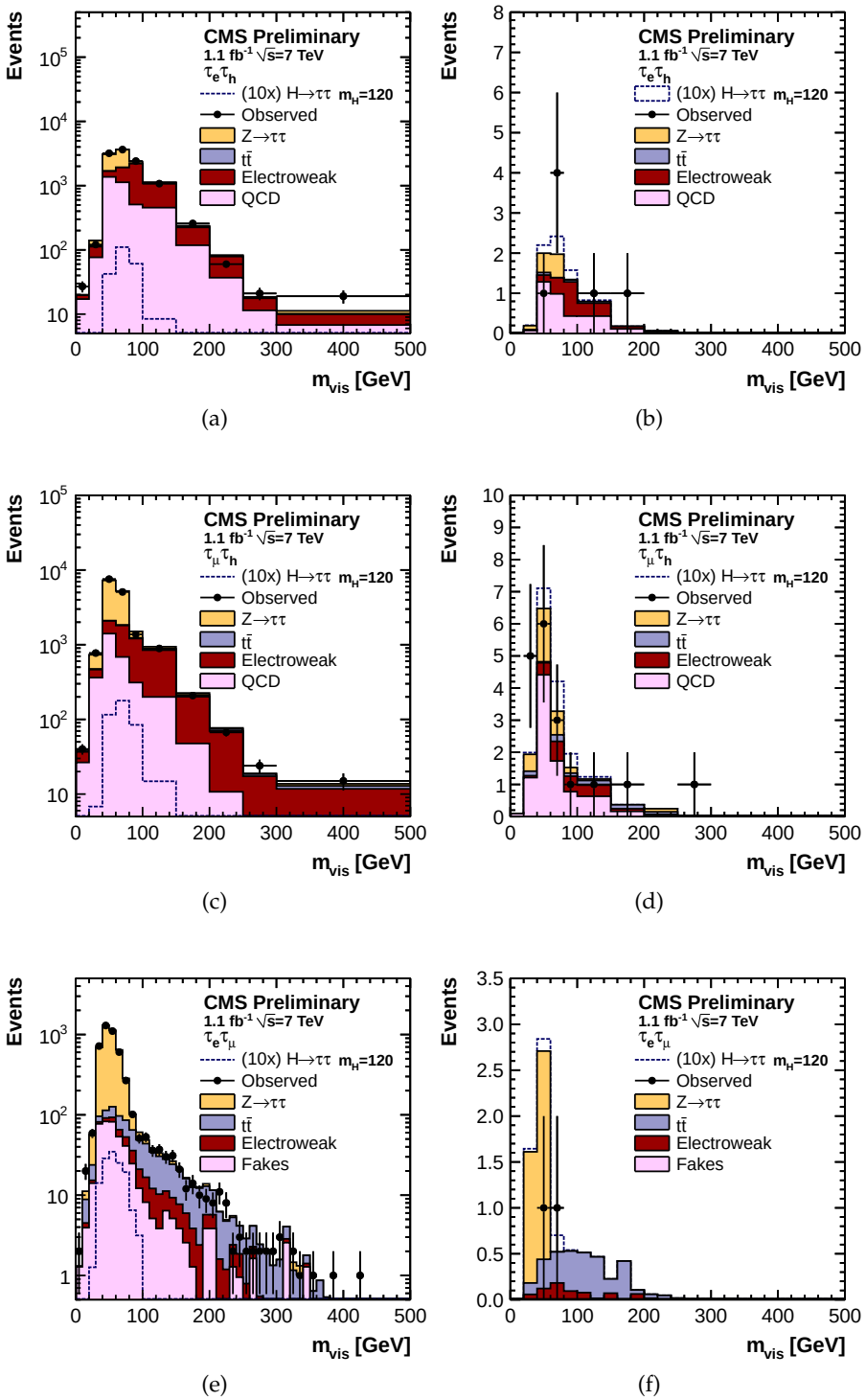

Figure 4: Input distributions from the $H \to \tau\tau$ analysis for a SM Higgs boson with $m_H = 120$ GeV/c^2: visible mass distributions for (a) $e\tau_{had}$ and non-VBF selection, (b) $e\tau_{had}$ plus VBF selection, (c) $\mu\tau_{had}$ and non-VBF selection, (d) $\mu\tau_{had}$ plus VBF selection, (e) $e\mu$ and non-VBF selection, (f) $e\mu$ plus VBF selection. The observed data are shown with points, while the expected background and signal rates are represented by histograms. Signal is multiplied by a factor of 10, to be better visible. Normalizations for all backgrounds are obtained using data-driven techniques.

3.3 $H \to bb$ channel [13]

We search for the associated production of the Higgs with W or Z bosons with the Higgs decaying to $b\bar{b}$ pairs. The analysis is performed in a data sample corresponding to an integrated luminosity of 1.1 fb^{-1}. The following final states are included: $W(\mu\nu)H$, $W(e\nu)H$, $Z(\mu\mu)H$, $Z(ee)H$ and $Z(\nu\nu)H$ —all with the Higgs decaying to $b\bar{b}$ pairs.

We used single and double lepton triggers that include isolation. The offline p_T (E_T) threshold for single muon (electron) channels was 20 (30) GeV. For di-lepton channels threshold was set at 20 GeV for each of the leptons. For $Z(\nu\nu)H$ we used triggers with large missing transverse energy E_T^{mis} with, and without, jets. The E_T^{mis} thresholds were > 80 and > 150 GeV, respectively.

Backgrounds arise from the production of W and Z bosons in association with jets (gluons and u, d, s, c, b quark flavors), singly and pair-produced top quarks, and dibosons. Simulated samples of all backgrounds are used to provide guidance in the optimization of the analysis cuts. These backgrounds overwhelm the VH signal by several orders of magnitude. The signal event selection is therefore tight and it aims to reconstruct kinematically the W/Z vector bosons and the Higgs decay into two b-jets, while also reducing the background significantly.

Candidate WH decays are identified by requiring the presence of a single, isolated, lepton and additional missing transverse energy. Candidate $Z(\ell\ell)H$ decays are reconstructed by combining isolated, opposite charge pairs of electrons and muons and requiring the dilepton invariant mass to satisfy $75 < m_{\ell\ell} < 105$ GeV. The reconstruction of the $H \to b\bar{b}$ decay is made by requiring the presence of two central ($|\eta| < 2.5$) particle-flow jets, above a minimum p_T threshold and tagged by the CSV (Combined Secondary Vertex) b-tagging algorithm [35]. If more than two such jets are found in the event, the pair with the highest sum of the CSV outputs for the two jets is chosen or the pair with highest di-jet p_T is chosen, depending on the mode.

The topology of VH production is such that the W/Z and the Higgs recoil away from each other with significant p_T. Cuts on the azimuthal opening angle between the vector boson and the reconstructed momenta of the Higgs candidate, on the p_T of the vector boson and on the b-tagged dijet pair achieve significant rejection for most background processes and improve the analysis reach. This "boost" requirement was > 160 GeV for $Z(\nu\nu)H$, > 150 GeV for WH, and > 100 GeV for $Z(\ell\ell)H$. For the $Z(\nu\nu)H$ channel, QCD backgrounds are further reduced by a factor of ~ 30 by requiring that the pfMET does not originate from mismeasured jets. A cut on the azimuthal angle (> 1.5 rad) between the pfMET and the closest jet is applied, together with the requirement that pfMET significance be > 5.

Appropriate high-purity control regions, orthogonal to the signal region, are identified in data for the most important backgrounds. Discrepancies between the expected and observed yields in the data in these control regions are used to obtain a scale factor by which the estimates from the simulation are adjusted. The background from these sources in the signal region are then estimated from the adjusted simulation samples, taking into account statistical and systematic uncertainties in the procedure.

An optimization of the event selection, that depends on the Higgs mass, is performed, and 95% C.L. upper limits on the $pp \to VH$ production cross section, relative to the standard model prediction, are obtained for Higgs masses between 110 and 135 GeV. These limits are based on the observed event count and background estimate in signal regions defined in the output discriminant of a boosted decision tree algorithm. This algorithm enhances the statistical power of the analysis by making full use of correlations between discriminating variables in signal and background events.

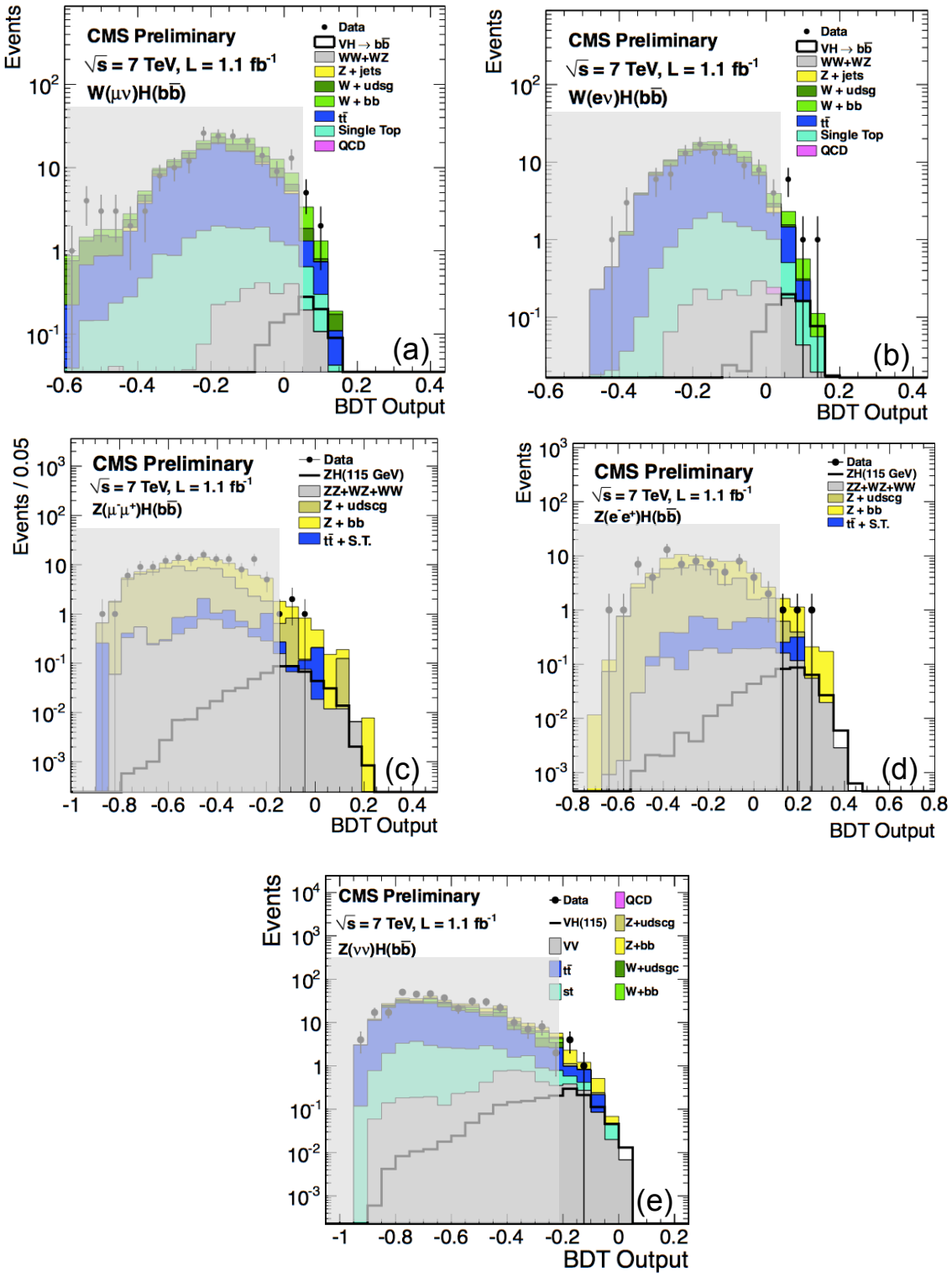

Figure 5: BDT output distributions for the $H \to bb$ analysis for a SM Higgs boson with $m_H = 115\,\mathrm{GeV}/c^2$: (a) $WH \to e\nu(bb)$, (b) $WH \to \mu\nu(bb)$, (c) $ZH \to ee(bb)$, (d) $ZH \to \mu\mu(bb)$, (e) $ZH \to \nu\nu(bb)$. The observed data are shown with points, while the expected background and signal rates are represented by histograms. Normalizations for the main contributing backgrounds are absolute, and are obtained using data-driven techniques. The faint areas cover the part of the BDT output that has a small signal-to-background ratio and is not used in the statistical analysis.

3.4 $H \to WW \to 2\ell 2\nu$ channel [14]

In this channel, we search for events with two oppositely charged leptons and large missing energy arising from neutrinos in W-decays. The search is based on the cut-and-count approach.

Events are collected using single and di-lepton triggers. In the offline analysis of recorded data, we consider muons with $p_T > 10$ GeV/c and $|\eta| < 2.4$ and electrons with $p_T > 10$ GeV/c and $|\eta| < 2.5$. We require there to be two oppositely-charged, isolated leptons, in three final states: e^+e^-, $\mu^+\mu^-$, or $e^\pm\mu^\mp$. Both leptons are required to be isolated. Electrons originating from photon conversions are suppressed by requiring no missing hits along their trajectory in the pixel detector and a low probability of the conversion vertex fit. Events with more than two high-p_T leptons are rejected in order to reduce the WZ and ZZ backgrounds.

To help suppress the $t\bar{t}$ background, events with additional soft muons are vetoed. We also veto events with b-tagged jets. Events with two same-flavor leptons forming an invariant mass within ± 15 GeV/c^2 around the pole Z-boson mass are rejected (Z-veto). To further suppress the Drell-Yan background, we require that the projection of the missing tranverse energy onto the direction transverse to the nearest lepton must be greater than 40 (20) GeV for same-flavor (opposite-flavor) di-lepton events. We also veto events where the di-lepton system is found to approximately recoil against a leading jet with $E_T > 15$ GeV, i.e. events with $\Delta\phi_{\ell\ell,jet} > 165^\circ$.

Finally, events are classified by the presence of 0, 1, or 2 jets with $p_T > 30$ GeV/c and $|\eta| < 5.0$. The 0- and 1-jet bin categories are further split into same-flavor (SF) and opposite-flavor (OF) groups. Hence, the current analysis is based on 5 independent sub-channels.

To help separate $H \to WW$ from the electroweak WW di-boson production, we exploit the scalar nature of the Higgs boson resulting in two leptons emitted preferably in one direction and with a smaller invariant mass compared to the non-resonant WW production. Hence, extra requirements are placed on the transverse momenta of the harder and the softer leptons, the dilepton mass, and the azimuthal angle difference between the two selected leptons. The transverse invariant mass m_T of the two leptons and missing tranverse energy E_T^{mis} has information on the Higgs boson mass and is also used for mass dependent two-sided cuts.

For the two-jet bin, in addition to the basic selection described earlier, we require the two jets to have VBF-like kinematics: exactly 2 jets with $m_{jj} > 450$ GeV/c^2 and $|\Delta\eta_{jj}| > 3.5$.

The four m_T-distribution for the $m_H = 160$ GeV/c^2 analysis in the zero-jet and one-jet bins, together with the $|\Delta\eta_{jj}|$ distribution for the 2-jet bin, are shown in Figures 6 and 7. The hatched areas shown in these plots have a low signal-to-background ratio and are rejected.

After all selection cuts are applied, the main backgrounds are: W^+W^- continuum, $t\bar{t}$, Drell-Yan, W+jets, and WZ/ZZ. All the main backgrounds are evaluated using the following data-driven techniques.

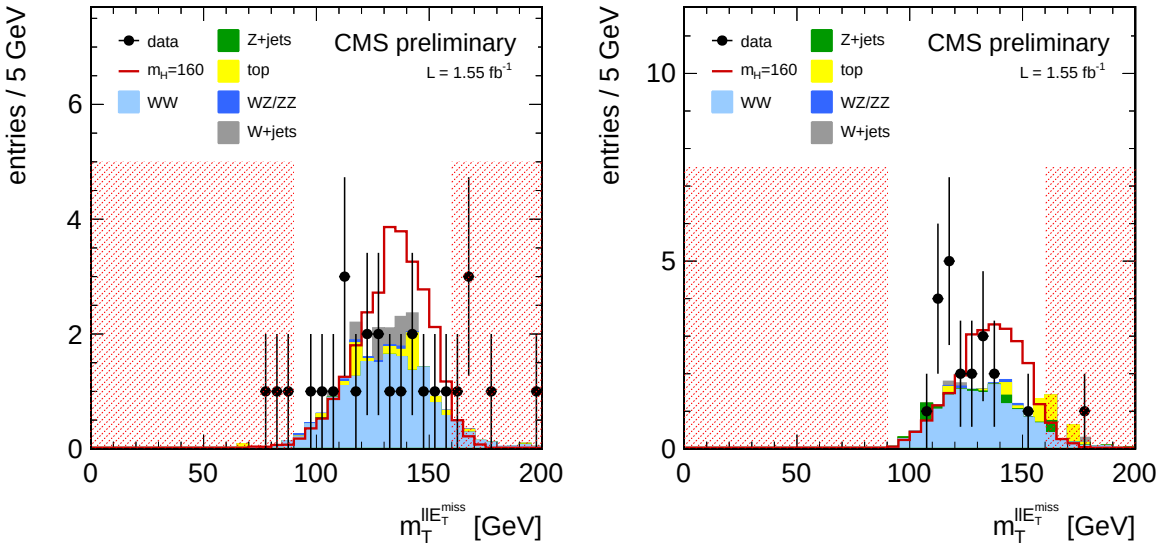

(a) (b)

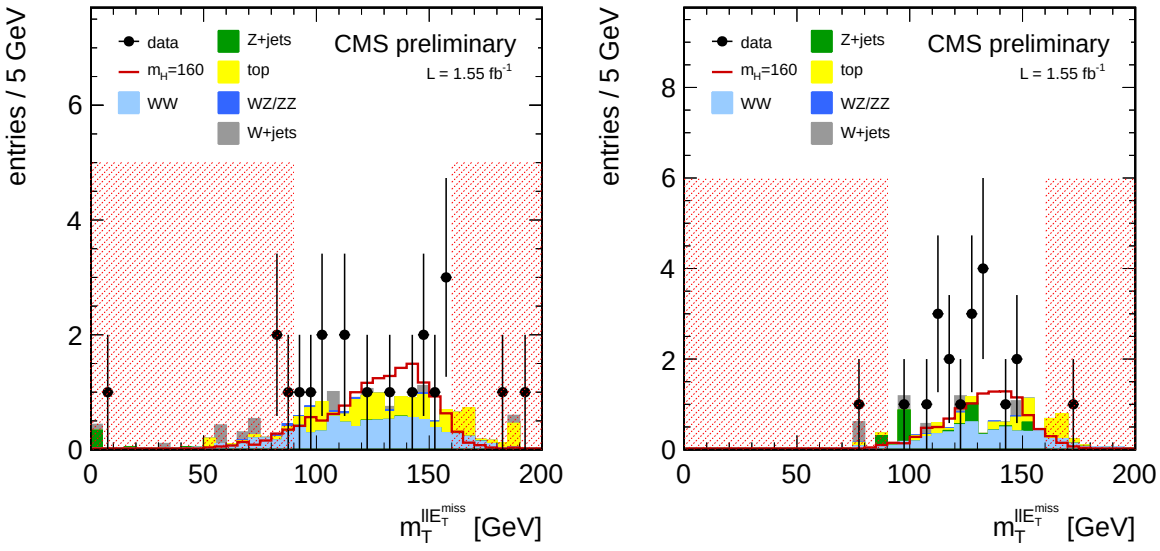

(c) (d)

Figure 6: Input information from the $H \to WW \to 2\ell 2\nu$ analysis for a SM Higgs boson with $m_H = 160\,\mathrm{GeV}/c^2$: (a) m_T distribution for $e\mu$ events with no jets, (b) m_T distribution for ee and $\mu\mu$ events with no jets, (c) m_T distribution for $e\mu$ events with 1 jet, (d) m_T distribution for ee and $\mu\mu$ events with 1 jet. The observed data (points) and expected background and signal rates (histograms) are shown. Normalizations for the WW, $t\bar{t}$, W+jets, and Drell-Yan background predictions are obtained using data-driven techniques. The areas hatched out in the plots are not used.

The $t\bar{t}$ background is estimated by extrapolation from the observed number of events with the b-tagging cut inverted. The Drell-Yan background measurement is based on extrapolation from the observed number of e^+e^-, $\mu^+\mu^-$ events with the Z-veto cut inverted. The background W+ jets and QCD multi-jet events is derived from measuring the number of events with one lepton passing a loose cut on isolation. The probabilities for such loosely-isolated fake leptons to pass tight isolation cut are measured in data using multi-jets events. The dominating systematic uncertainty is the difference between the prediction of W+ jets yield and the prediction on simulation using this method (closure test).

The non-resonant WW contribution for low mass signal region, $m_H \leq 200$ GeV/c^2, is estimated using events with a di-lepton mass larger than 100 GeV/c^2, where there is a negligible contamination from the Higgs boson signal. For larger Higgs boson masses there is a large overlap between the non-resonant WW background and a Higgs boson signal and we thus use simulation.

The largest uncertainties on the signal yield include theoretical errors on total cross sections (5-15%), acceptance for exclusive 0/1/2-jet final states (7-20%), and integrated luminosity (4.5%). The largest background systematic errors come from statistical uncertainties in the number of events observed in the control samples (20-60%), Monte Carlo statistical errors limiting the accuracy with which we can validate the data-driven techniques (10-20%), and from application of the lepton fake rate estimation to W+jets control sample (36%).

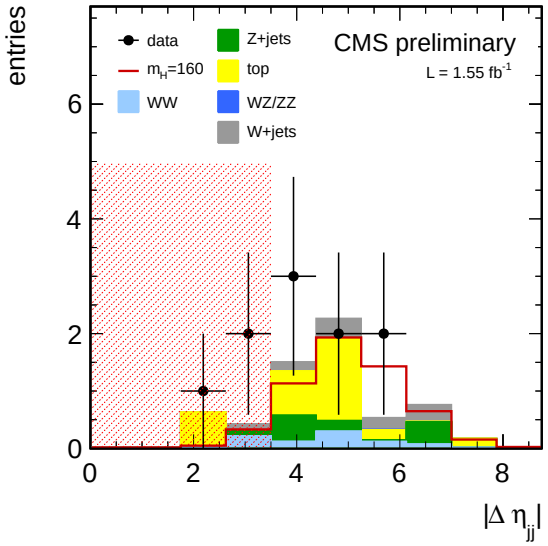

(a)

Figure 7: Input information from the $H \to WW \to 2\ell 2\nu$ analysis for a SM Higgs boson with $m_H = 160$ GeV/c^2: $|\Delta\eta_{jj}|$ distributions for 2ℓ events with 2 jets. The area with low values of $|\Delta\eta|$, hatched out in the plot, are not used. The observed data (points) and expected background and signal rates (histograms) are shown.

3.5 $H \to ZZ \to 4\ell$ channel [15]

In this channel, we search for a narrow resonance peaked over the continuum of the four-lepton mass $m_{4\ell}$ distribution. The number of observed events is very low and we use the unbinned approach. The analysis is performed in three sub-channels: $4e$, 4μ, $2e2\mu$.

Events used in the analysis have been collected by di-lepton triggers at low and high luminosities, respectively. To be considered in the offline analysis, electrons are required to have $p_T > 7$ GeV/c and $|\eta| < 2.5$ and muons must have $p_T > 5$ GeV/c and $|\eta| < 2.4$. Also, such leptons must be isolated in the tracking and calorimeter detectors and must not have large significance of the 3D impact parameters with respect to the common vertex. In events with four or more leptons, we ask for at least one pair of same-flavor, opposite-charge di-leptons satisfying the following cuts: $p_T^{max} > 20$ GeV/c, $p_T^{min} > 10$ GeV/c, $60 < m_{\ell\ell} < 120$ GeV/c^2. If more than one pair satisfies this requirement, the one with the invariant mass closest to the Z-boson mass is picked. The second pair of same-flavor, opposite-charge leptons must form an invariant mass $20 < m_{\ell\ell} < 120$ GeV/c^2. If more than one four-lepton combination satisfies all the criteria, then the one with the highest p_T leptons is chosen. Four leptons selected in such a process form a ZZ event candidate with a mass $m_{4\ell}$.

Fig. 8 shows observed events as well as parametric density functions for the expected backgrounds and signal for a Higgs boson mass of $m_H = 300$ GeV/c^2.

The signal shape $f_S(m_{4\ell})$ is constructed as the Breit-Wigner function convoluted with the detector four-lepton mass resolution modeled with the crystal ball function. Default parameters are derived from fitting simulated Higgs events, which were generated using the next-to-leading-order (NLO) matrix-element generator POWHEG [31] interfaced to PYTHIA [32] for parton showering and passed through the full detector simulation.

The dominant irreducible background is the electroweak ZZ-production. The mass shape for this background is known at NLO and further corrected to include the contribution of $gg \to ZZ \to 4\ell$. Both the NLO $m_{4\ell}$ shape and an additional gg-correction were evaluated with MCFM [36]. To reduce systematic errors associated with integrated luminosity and lepton reconstruction/identification efficiencies, the overall event yield of the ZZ-background is obtained by scaling the observed numbers of Z-events in the $2e$- and 2μ-channels by the theoretical ratio of ZZ of Z cross sections. The reducible backgrounds $Z + jets$ (including heavy flavor jets) and $t\bar{t}$ are evaluated from the data, relying on the inversion of the isolation and impact parameter cuts—their contribution is estimated to be almost negligible.

The main sources of systematic errors on signal and irreducible backgrounds are due to theoretical uncertainties on their cross sections: 6% (QCD scales) and 8% (PDF) for Higgs and 7% (combined) for ZZ. For Higgs boson masses $m_H > 300$ GeV/c^2, theoretical uncertainties on the virtual Higgs mass lineshape may become large; however, for a lack of a model for such uncertainties, they are not included in these preliminary results. Trigger, lepton reconstruction, and isolation cut efficiencies for prompt leptons are derived from data using $Z \to ee$ and $Z \to \mu\mu$ events (tag-and-probe method) with the net uncertainty on the event yields of about 1-3%.

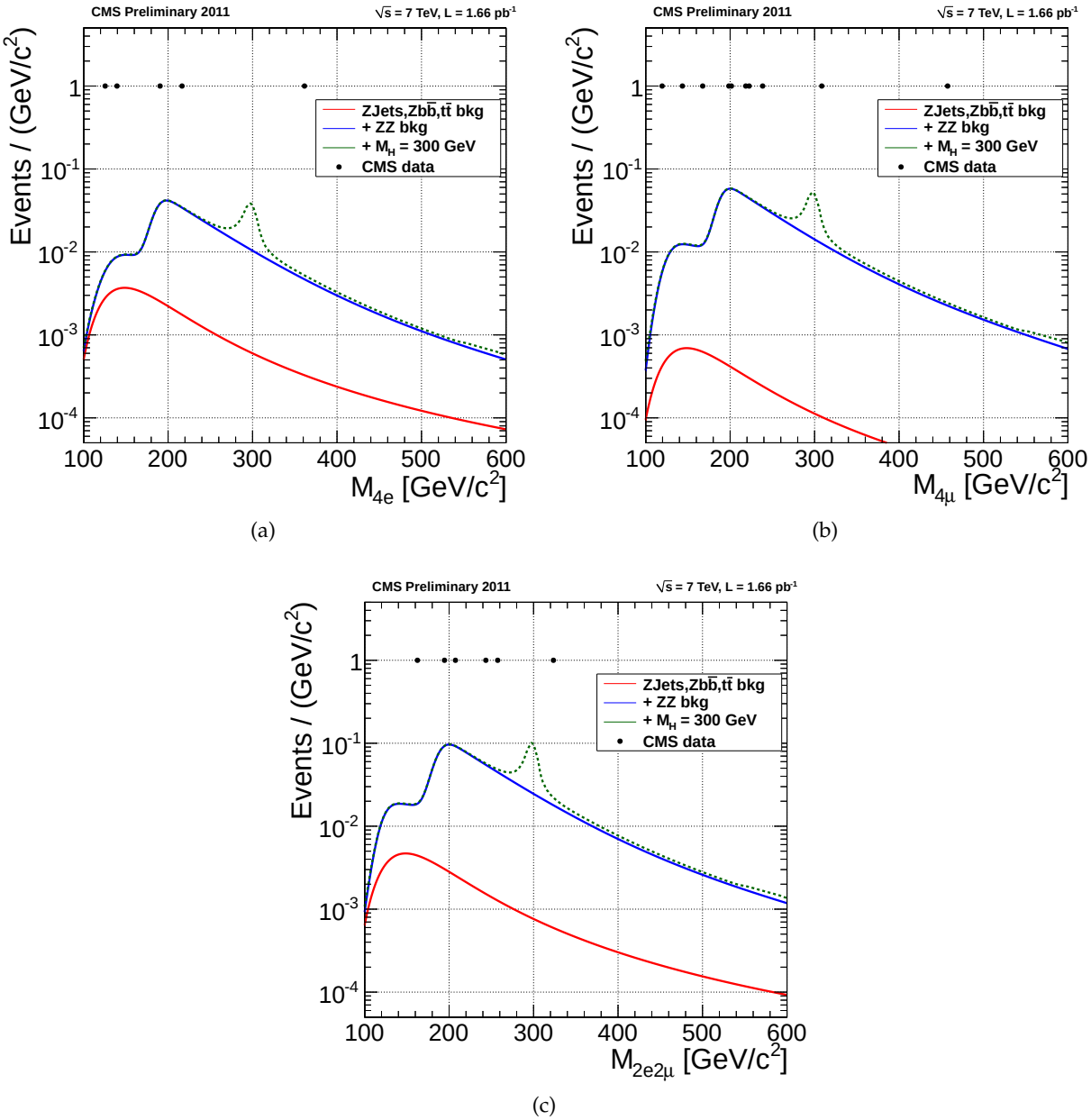

(a) (b)

(c)

Figure 8: Input information from the $H \to ZZ \to 4\ell$ analysis for a SM Higgs boson with $m_H = 300$ GeV/c^2: $m_{4\ell}$ mass distributions for (a) $4e$, (b) 4μ, and (c) $2e2\mu$ final states. The observed events are indicated by square symbols. The curves show parametric density functions for the expected background and signal rates. Normalization for reducible backgrounds is obtained using data-driven techniques.

3.6 $H \to ZZ \to 2\ell 2\tau$ channel [16]

In this channel, we search for a narrow resonance peaked over the continuum four-lepton mass $m_{2\ell 2\tau}$ distribution. The events selected for this analysis pass triggers which require the presence of at least two muons or electrons in the event with transverse momentum $p_{\mathrm{T}} > 13(8)$ GeV for leading (subleading) muons and $p_{\mathrm{T}} > 17(8)$ GeV for electrons.

One Z, which is called "leading", is required to decay into $\mu\mu$ or ee pairs, whereas the second Z decays into $\tau\tau$ with four possible final states: $\tau_{\mathrm{h}}\tau_{\mathrm{h}}$, $\mu\tau_{\mathrm{h}}$, $e\tau_{\mathrm{h}}$ and $e\mu$, where τ_{h} represents hadronically decaying taus. The leading Z boson candidate must have leptons of opposite charge with p_T greater than 20 GeV and 10 GeV for leading and subleading leptons, respectively, and satisfy $|\eta| < 2.4$ for muons and $|\eta| < 2.5$ for electrons. For the subleading Z boson, a tau pair is selected. Since taus decay both leptonically and hadronically the muons and electrons are required to have p_{T} in excess of 10 GeV, the taus are required to have $p_{\mathrm{T}} > 20$ GeV, pseudorapidity $|\eta| < 2.3$. Since only visible tau decay products are used, the invariant mass of the reconstructed $Z \to \tau\tau$ should be between 30 and 80 GeV.

Figure 9 shows observed events as well as expected backgrounds and signal for Higgs boson masses of $m_H = 200$ GeV/c^2 and $m_H = 400$ GeV/c^2, which were generated using the next-to-leading-order (NLO) matrix-element generator POWHEG [31] interfaced to PYTHIA [32] for parton showering and passed through the full detector simulation.

The background shapes taken from the MC simulation were normalized using data driven methods. The amount of the ZZ contribution was estimated in a data–driven way by scaling to the well–measured inclusive Z production cross-section. The ZZ cross-section was calculated at NLO and includes the $gg \to ZZ$ contribution both evaluated with MCFM [36]. The background contributions from Z and WZ production with associated jets, $t\bar{t}$ and QCD multijet production were estimated simultaneously. In all the cases, a jet or non-isolated lepton can be misidentified as a τ_{h}. The probability for jets to fake a τ_{h} was measured using events in which the leading Z passed all selection requirements and τ_{h} pairs are observed, where no requirement on the τ_{h} isolation is applied. Additionally, the two τ_{h} candidates are required to have the same charge. To estimate the number of background events in the signal region, the measured fake–rate is applied to events which pass all selection requirements, including proper charge combination of the subleading Z, but requiring the τ_{h} candidates to be anti-isolated.

The main sources of systematic errors on signal and irreducible backgrounds are due to theoretical uncertainties on their cross sections: 6% (QCD scales) and 8% (PDF) for Higgs and 7% (combined) for ZZ. Trigger, lepton reconstruction, and isolation cut efficiencies for prompt leptons are derived from data using $Z \to ee$ and $Z \to \mu\mu$ or $Z \to \tau\tau \to \mu\tau$ events (tag-and-probe method) with the net uncertainty on the event yields of about 1-4%. The tau identification uncertainty is 6-7% and the energy scale uncertainty, 3%.

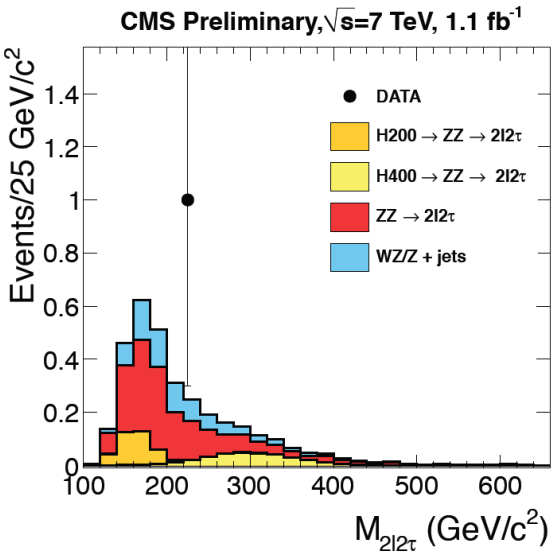

Figure 9: Invariant mass distribution of the $\ell\ell\tau\tau$ system in the $H \to 2\ell 2\tau$ analysis for a SM Higgs boson with $m_H = 200$ and 400 GeV/c^2. The tau leptons include both hadronic and leptonic decays (no overlaps with the $H \to ZZ \to 4\ell$ signature are allowed). The observed event is shown with a point, while the expected background and signal rates are represented by histograms. Background contributions are stacked, while the SM Higgs boson signal is shown superimposed. Given the very low expected event yield with the current integrated luminosity, all eight independent $\ell\ell\tau\tau$ final states used in the search are added together on this plot.

3.7 $H \to ZZ \to 2\ell 2\nu$ channel [17]

In this channel, the search is performed using a cut-and-count approach and two sub-channels: $2e2\nu$, $2\mu 2\nu$.

Events are selected using double-lepton triggers. The two leptons are required to pass all prompt lepton identification cuts (basic identification, isolation, impact parameter), satisfy kinematic cuts, and form an invariant mass in a ± 15 GeV/c^2 mass window around m_Z, and have $p_T(\ell\ell) > 25$ GeV/c. Furthermore, cuts on the missing transverse energy MET, M_T (defined in footnote [3]), and $\Delta\phi(MET, jet)$ are applied to suppress a huge reducible background of $Z + jets$. MET, M_T, and $\Delta\phi(MET, jet)$ cuts depend on the Higgs boson mass being searched for. To help suppress the $t\bar{t}$ and single-top -backgrounds, events with b-tagged jets are vetoed. Figure 10 shows the final M_T distributions for the two sub-channels before the M_T cut is applied.

The ZZ and WZ backgrounds are taken from Monte Carlo simulation. The WZ background cross section is calculated at NLO. The ZZ background is a combination of NLO ZZ and $gg \to ZZ$, known at LO.

The Z+jets background has a very large cross section and is suppressed by the analysis cuts with an efficiency $O(10^{-5})$. To estimate the remaining rate of Z+jets events, we rely on the data-driven technique taking advantage that $Z(\ell\ell)$+jets and γ+jets are very closely related, while the latter has a much higher observable event yield.

The *non-resonant* backgrounds, i.e. those without Z-boson (mostly, $t\bar{t}$ and WW), are also derived from data, taking advantage that non-resonant backgrounds, in addition to e^+e^- and $\mu^+\mu^-$, also, give $e^\pm\mu^\mp$ events.

The main sources of systematic errors on signal and irreducible backgrounds are due to theoretical uncertainties on their cross sections (up to 15% for Higgs, 7.8% for $qq \to ZZ$ and 20% for $gg \to ZZ$). The main uncertainties for backgrounds are coming from the methods used to measure the backgrounds from data - the channel is characterized by tight cuts and little populated phase space, therefore methods as of now are limited by statistics available (with typical uncertainty 50%).

[3] M_T is defined as follows: ${M_T}^2 = (\sqrt{{P_{TZ}}^2 + {M_Z}^2} + \sqrt{{MET}^2 + {M_Z}^2})^2 - (\vec{P_{TZ}} + \vec{MET})^2$.

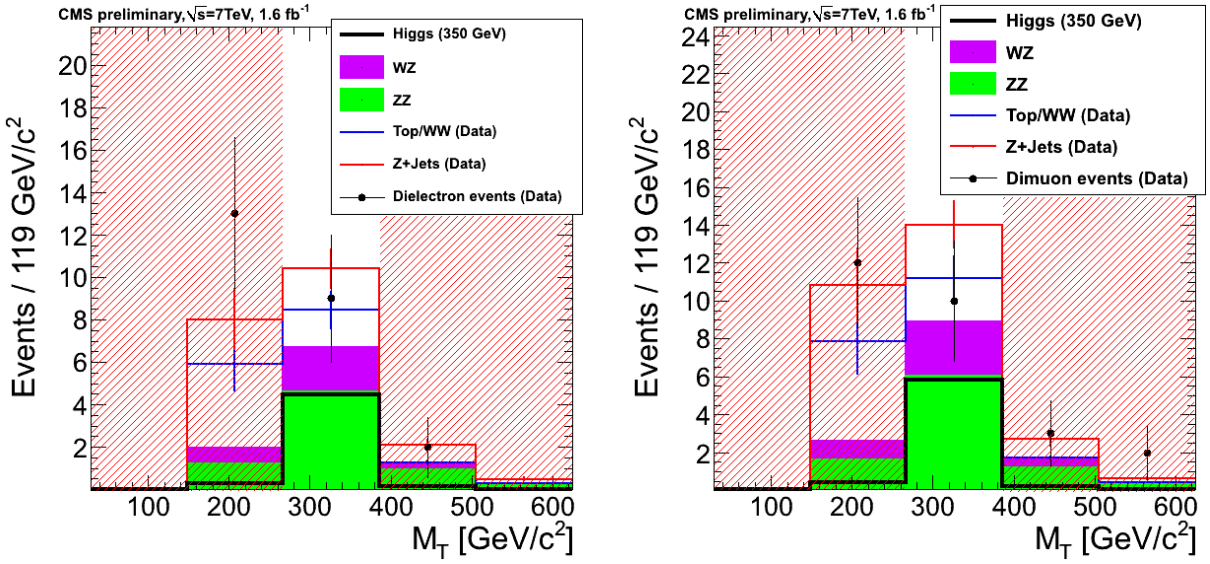

(a) (b)

Figure 10: M_T distributions for (a) $Z_{ee} + MET$ and (b) $Z_{\mu\mu} + MET$ events with cuts optimized for a search of the standard model Higgs boson with mass $m_H = 350$ GeV$/c^2$. The observed data (points) and expected background and signal rates (histograms) are shown. Background contributions are stacked, while the SM Higgs boson signal is shown superimposed. Some of the backgrounds are obtained using data-driven techniques as indicated on the plots. Only the bin not covered by the hatched area was used in the statistical analysis of data for the given Higgs boson mass.

3.8 $H \to ZZ \to 2\ell 2q$ channel [18]

The Higgs boson search in the channel $H \to ZZ \to 2\ell 2q$ proceeds by searching for a peak in the invariant mass of the dilepton plus dijet system m_{ZZ}. The width of the peak is affected by the jet energy resolution and is improved by constraining the dijet invariant mass to the Z boson mass.

The main sources of background are $Z + jets$ and a small contribution of $t\bar{t}$ and electroweak diboson production. Leptons are required to be isolated and to pass quality requirements. The leading lepton must have $p_T > 40$ GeV/c and the other one $p_T > 20$ GeV/c. All jets are required to have $p_T > 30$ GeV/c. In order to further reduce the amount of background, requirements on dijet and dilepton invariant masses are applied: $75 < m_{jj} < 105$ GeV/c^2 and $70 < m_{\ell\ell} < 110$ GeV/c^2. Events are categorized in different exclusive channels according to the lepton flavour ($2e2q$ and $2\mu 2q$) and according to the number of b-tagged jets (zero, one, or two b-tagged jets). Further background rejection is achieved by exploiting the different angular distribution of Higgs boson signal with respect to background and applying a quark-gluon discriminator in the category with no b-tagged jets, which is the most affected by $Z + jets$ background. To help suppress $t\bar{t}$ background in the category with 2 b-tagged jets, a cut on missing transverse energy significance is also used.

The statistical analysis is based on the m_{ZZ} distribution. The background shape and normalization are determined from data using the m_{ZZ} distribution in the sidebands obtained by inverting the m_{jj} requirement using an unbinned maximum likelihood fit. The signal shape is described by a relativistic Breit–Wigner convoluted with a Crystal-Ball function determined from simulation. The signal reconstruction efficiency and the resolution function are parameterized as a function of the hypothetical Higgs boson mass.

Figure 11 shows the observed data, the expected background, as derived from an independent data control sample, and an example of the expected signal.

The main sources of systematic uncertainty affecting the signal yield are the uncertainties on the total cross section and branching ratio, ∼17%, and the integrated luminosity, ∼4.5%. The uncertainty on b-tag efficiency can vary from 1% to 20% depending on the category. Effects from lepton energy scale, muon and electron reconstruction efficiency, jet resolution and efficiency, pile-up, quark-gluon discrimination, E_T^{miss} and production mechanism are considered as well.

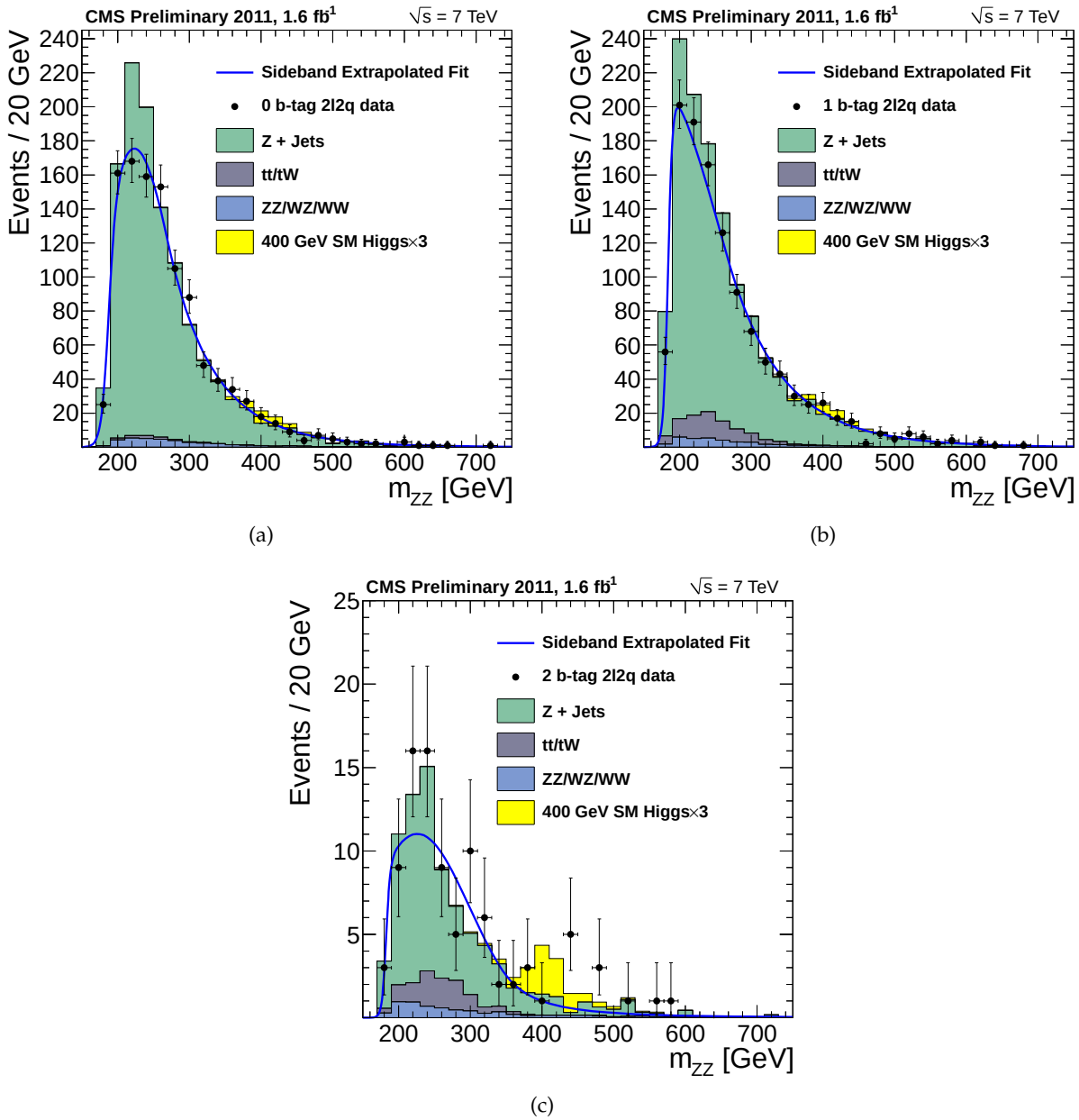

(a) (b)

(c)

Figure 11: Binned $m_{2\ell 2j}$ distributions for: (a) 2ℓ+2 jets, with 0 b-tags, (b) 2ℓ+2 jets, with 1 b-tag, (c) 2ℓ+2 jets, with 2 b-tag. The $2e$ and 2μ final states are combined together here, but in the overall statistical analysis they are treated separately. The line corresponds to the background model, whose shape and normalization are derived from independent control samples. Monte Carlo generated background distributions are shown only for comparison—they are not used directly in the statistical analysis. The expected SM Higgs boson signal, multiplied by a factor of 3, for $m_H = 400\,\text{GeV}/c^2$ is also shown. Although the data are shown as binned distributions, the actual analysis is carried out unbinned.

4 Higgs search results

4.1 Summary and discussion of results obtained in the individual analyses

None of the searches performed in the eight channels entering the overall combination shows an excess of events that we believe is significant. Limits on the signal strength modifier, $\mu = \sigma/\sigma_{SM}$, as obtained individually in each of these searches are shown in Figs. 12- 19. The solid lines denote the experimentally observed limits and the dashed lines, the median expected limits for the background-only hypothesis. The solid color bands indicate the possible variation in the expected limit in the background-only hypothesis, given the current statistical and systematic errors. The green (yellow) bands are expected to contain 68% (95%) of all excursions of the expected limit. As to be expected, some fluctuations in the limits extracted from the data are observed.

The top panel on the right hand side of Figs. 12-19 shows the observed p-values, indicating how much incompatible observed excesses are with the background-only hypothesis. However, p-values by themselves do not provide any information on whether observed excesses would be consistent with the SM Higgs boson hypothesis. The best fit value of $\hat{\mu}$ indicates by how much the SM Higgs cross section would need be scaled to make it consistent with an observed excess, and is shown in the lower right panels with a solid line. The light blue band indicates the $\pm 1\sigma$ range is obtained in the fit.

The expected limits on μ for the $H \to \gamma\gamma$ channel (Fig. 12) are of the order of 2-4 in the chosen range, but then deteriorate for $m_H < 110$ GeV/c^2 and $m_H > 150$ GeV/c^2 mostly due to the decrease in the branching ratio BR$(H \to \gamma\gamma)$ outside the 110-150 GeV/c^2 mass range and larger background at low masses. The observed limits exhibit some fluctuations with a correlation length characteristic of the average $\gamma\gamma$ mass resolution, ranging between approximately 1 and 3% for different di-photon categories. The minimum p-value of the largest excess is about 0.0025 ($Z_{max} = 2.8\sigma$). Taking into account the look-elsewhere effect, evaluated by generating pseudo-data for the background-only hypothesis, the chance of observing a maximum excess as large as seen in the data is about 0.05 ($Z_{global} \sim 1.7\sigma$), giving the trials factor O(20).

The limits obtained with the $H \to \tau\tau$ channel (Fig. 13) do not have pronounced modulations, which stems from the $\tau\tau$ mass resolution being comparable to the explored range of Higgs boson masses. The degradation in the expected limit at higher masses results from the decrease in the branching ratio BR$(H \to \tau\tau)$ and the decreasing signal cross section. The observed limits are about 10 times the SM Higgs boson cross section and are consistent with the expectation.

The $H \to bb$ channel (Fig. 14) shows a very similar structure, with a slight excess of events, fully compatible with statistical fluctuations. The degradation in the expected limit at higher masses results from the decrease in the branching ratio BR$(H \to bb)$ and the decreasing signal cross section $pp \to VH$. The observed limits are about 10 times the SM Higgs boson cross section and are consistent with the expectation.

The $H \to WW \to 2\ell 2\nu$ channel (Fig. 15) provides limits on values of μ less than the SM expectation around $m_H = 160$ GeV/c^2, where BR$(H \to WW) \sim 100\%$. At lower masses, the branching ratio falls very quickly. At higher masses, while the branching ratio remains fairly high, the signal cross section falls and the expected limits deteriorate. The observed limits in the low mass range below 180 GeV/c^2 show a broad $\sim 1\sigma$ upward deviation. This observed excess weakens the limits that we set in this mass range. Since in this analysis one does not have a direct measure of the Higgs boson mass, the correlation length for excursions of the observed limit and p-value curves is large and estimated to be ± 30 GeV/c^2 in the low mass range by injecting signal Monte Carlo events into pseudo-data, which resulted in broad excesses over

a 50-80 GeV/c^2 mass range. Fluctuations of the number of background events would also appear as similarly broad "low frequency" excursions of the observed limit curve away from the median expected. The overall look-elsewhere effect is small.

The $H \to ZZ \to 4\ell$ channel (Fig. 16) has a very characteristic structure in the expected limits that mirrors the dependence of the branching ratio BR($H \to ZZ$) on the Higgs boson mass. The worsening limits at high masses come from the decreasing signal cross section. The reduced sensitivity around $m_H = 160$ GeV/c^2 and for low masses comes from the very small $H \to ZZ$ branching ratio in these regions. The overall background rate, dominated by the electroweak ZZ di-boson production, is very low. The four-lepton mass resolution is very good, on the order of 1%. Therefore, the structure in the observed limits basically follows the distribution of the observed events (see Fig. 8). The total number of events with $m_{4\ell} > 100$ GeV/c^2 is 21, while 21.2 ± 0.8 events are expected from standard model background processes. Six of the events are below the kinematic threshold of two on-shell Zs ($mH < 180$ GeV/c^2), which is higher than the expected 2.8 ± 0.2. These six events form roughly three pairs around 120, 140, and 160 GeV/c^2, ruling out a common narrow source such as a SM-like signal. The $\hat{\mu}$ scan shows that the two dips of p-value around $m_H \sim 120$ and 160 GeV/c^2 would require a much stronger signal than the SM Higgs boson, while the two events around 140 GeV/c^2 are not inconsistent with the SM Higgs. The minimal p-value observed is $\sim$0.01. However, the look-elsewhere effect, estimated to be about 35 in the current search, washes out the level of significance of the dips we see in the p-value scan.

The $H \to ZZ \to 2\ell 2\tau$ channel has a sensitivity to exclude a signal with about 10 times the SM Higgs boson cross section (Fig. 17). For m_H below 200 GeV/c^2, the branching ratio and reconstruction acceptance of the di-tau system quickly decreases resulting in the rapid deterioration of the search sensitivity.

The expected limits for $H \to ZZ \to 2\ell 2\nu$ and $H \to ZZ \to 2\ell 2q$ channels have a typical concave structure (Figures 18 and 19). As one moves toward the lower masses, the Z+jets background quickly overwhelms a potential signal. Cuts optimized for a higher Higgs boson mass allow one to suppress this formidable background, but eventually the signal cross section becomes too small and limits worsen. The observed limits in these two channels fluctuate, as expected, with an absolute scale and "correlation length" consistent with expectations.

4.2 Combination results: search for the SM Higgs boson

The results of combining all eight analyses discussed in the previous section into one grand search for the SM Higgs boson are presented in Figures 20–24.

Figure 20 shows the CL_s value for the SM Higgs boson as a function of its mass. The observed values are shown by the solid line. The dashed line indicates the median expected value of CL_s, while the green/yellow bands indicate the $\pm 1\sigma$ (68%) and $\pm 2\sigma$ (95%) ranges in which the observed results are expected to reside for the *background-only* hypothesis. We exclude the SM Higgs boson at 95% C.L. in the three mass ranges 145-216, 226-288, and 310-400 GeV/c^2. This substantially reduces the allowed mass range for the SM Higgs boson that has remained unrestricted by the past LEP [7] and ongoing Tevatron [8] direct searches, as well as in comparison to the limits reported by the CMS and ATLAS Collaborations at the EPS conference [37, 38].

The expected exclusion, in the absence of a signal, is from 130-440 GeV/c^2. The two gaps between the three excluded mass ranges observed in data are consistent with statistical fluctuations. The observed CL_s values are about 2σ larger than the expectation in the mass range < 150 GeV/c^2, which makes the observed limits in this range less restrictive than expected. The

real significance of the excess, taking into account the look-elsewhere effect, will be discussed below. At 90% C.L., we exclude the SM Higgs boson in the mass range from 144-440 GeV/c^2, without interruptions.

The combined 95% C.L. upper limits on the signal strength modifier $\mu = \sigma/\sigma_{\rm SM}$ as a function of the Higgs boson mass are presented in Fig. 21. This plot shows by what factor the SM Higgs boson cross sections must be scaled to be excluded at 95% C.L. Filled points show the observed CL_s-based limits. The exclusion range for the SM Higgs boson ($\mu = 1$) is identical to that shown in Fig. 20. Naturally, the plots in Figs. 20 and 21 exhibit the same structure as they are basically different "representations" of intrinsically the same information. We also computed limits using the Bayesian method (with a flat prior) and obtained nearly identical results: out of the six borders of the three excluded regions, only one was affected, the difference with the CL_s results being 1 GeV/c^2.

Figure 22 shows the observed limits in the eight individual analyses and their combination. Both at low mass range below 160 GeV/c^2 and high mass range above 180 GeV/c^2, the combination depends on relative sensitivities of multiple analyses and the interplay of excesses and deficits seen in each of them. In other words, the combined limits sometimes are not necessarily better than the best single-channel limit. For Higgs boson masses from 160-180 GeV/c^2, the $H \to WW$ channel is the main contributor as this is the predominant decay mode in this range.

Figures 23 and 24 show a scan of the observed combined p-value as given by Eq. (9) vs. Higgs boson mass m_H . This scan characterizes how unlikely are the upward departures in the observed values of the test statistic q_0^{obs} approximately. One can see that the p-value curve dips downward over a broad range of low masses, driven by the excess seen in the WW-analysis, with a few narrower features corresponding to the $ZZ \to 4\ell$ events and modulations seen in the $H \to \gamma\gamma$ channel. The minimum local p-value is $p_{min} \sim 0.01$ and corresponds to the maximum local significance $Z_{max} = 2.3$. However, the look-elsewhere effect in this search is not negligible and has to be taken into account. It can be approximately assessed by counting the number of deficit-to-excess fluctuations N_0 across the entire search mass range as described in section 2. This corresponds to the number of times the p-value drops down below the $p = 0.5$ border line between excesses and deficits of events. Figure 23 (upper panel) shows six such p-value drops. Following Eq. 10, the global p-value to observe an excess with a significance $Z_{max} = 2.3$ is $p_{global} = p_{min} + N_0\, e^{-Z_{max}^2/2} \sim 0.4$.

The best-fit $\hat{\mu}$ value, also shown in Fig. 23 (lower panel) represents the factor by which the SM Higgs boson cross section has to be rescaled to agree with the data. For 140 GeV/c^2, the best fit for $\hat{\mu}$ is $\sim$0.6$\times$SM which is within 1σ of the expectation for a SM Higgs boson. Between 117 - 120 GeV/c^2, $\hat{\mu}$ is $\sim$1$\times$SM. However, as was discussed above, with the current amount of data, we believe that the excess is not significant.

Overall, the only definitive conclusion we can derive from the present search results are exclusion limits as reported above. More data, now rapidly coming, will increase the statistical accuracy of the existing analyses and allow us to introduce further improvements in search strategies, which will boost the sensitivity of our SM Higgs searches.

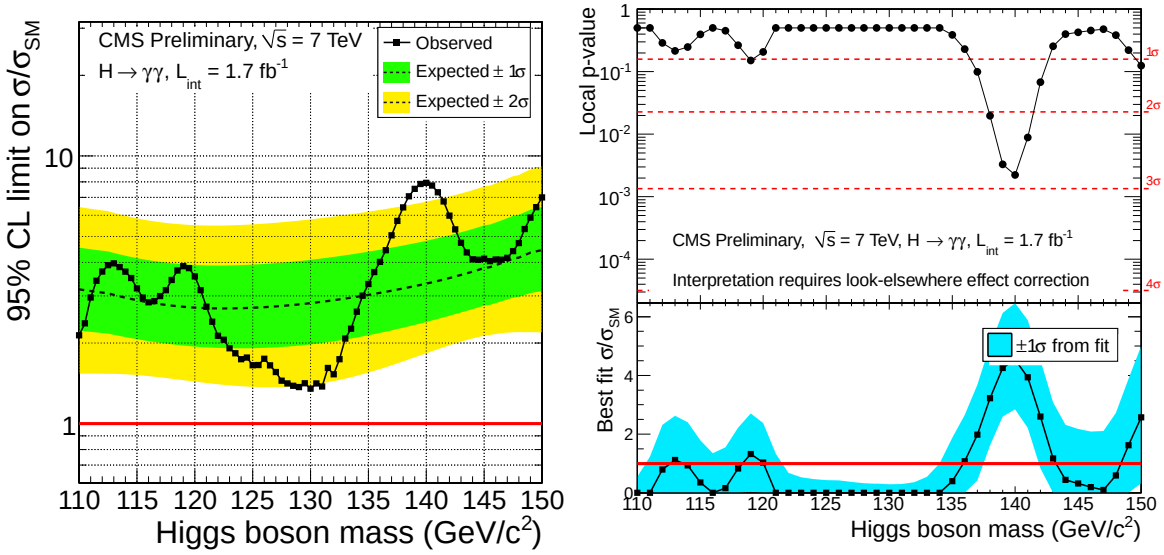

(a) (b)

Figure 12: $H \to \gamma\gamma$ analysis: (a) Limits on the signal strength modifier $\mu = \sigma/\sigma_{SM}$ vs. hypothesized Higgs boson mass m_H. (b) Local p-value (top panel) and best-fit signal strength $\hat{\mu}$ (bottom panel) vs. hypothesized Higgs boson mass m_H.

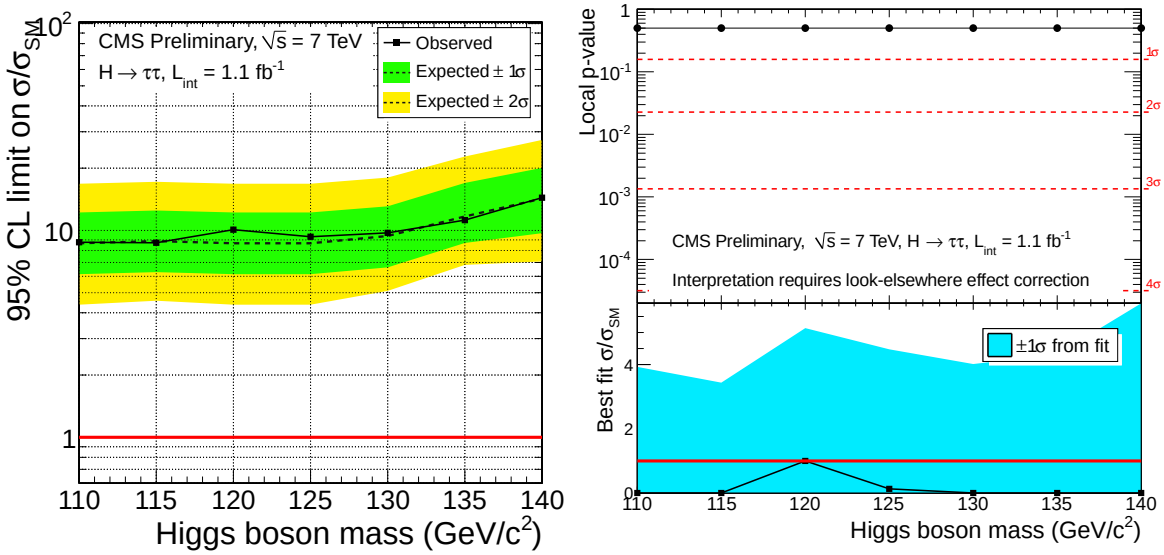

(a) (b)

Figure 13: $H \to \tau\tau$ analysis: (a) Limits on the signal strength modifier $\mu = \sigma/\sigma_{SM}$ vs. hypothesized Higgs boson mass m_H. (b) Local p-value (top panel) and best-fit signal strength $\hat{\mu}$ (bottom panel) vs. hypothesized Higgs boson mass m_H.

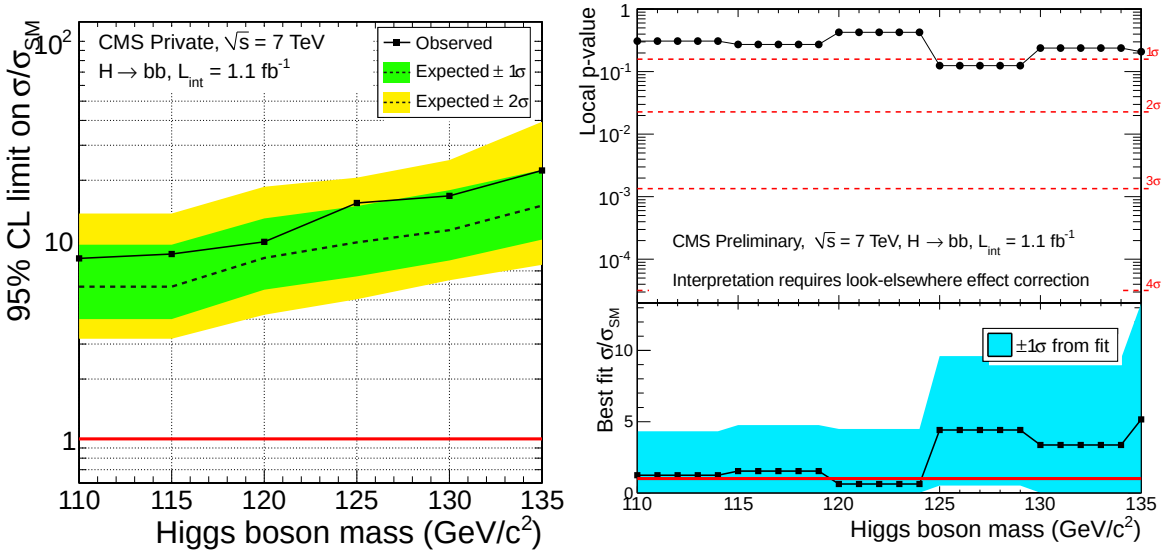

(a) (b)

Figure 14: $H \to bb$ analysis: (a) Limits on the signal strength modifier $\mu = \sigma/\sigma_{SM}$ vs. hypothesized Higgs boson mass m_H. (b) Local p-value (top panel) and best-fit signal strength $\hat{\mu}$ (bottom panel) vs. hypothesized Higgs boson mass m_H.

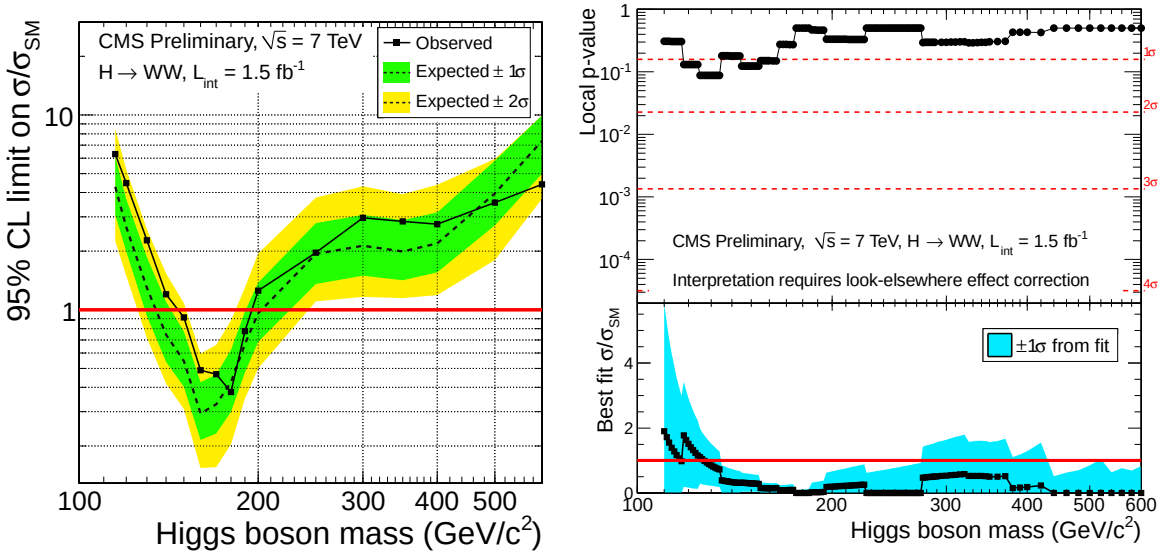

(a) (b)

Figure 15: $H \to WW \to 2\ell 2\nu$ analysis: (a) Limits on the signal strength modifier $\mu = \sigma/\sigma_{SM}$ vs. hypothesized Higgs boson mass m_H. (b) Local p-value (top panel) and best-fit signal strength $\hat{\mu}$ (bottom panel) vs. hypothesized Higgs boson mass m_H.

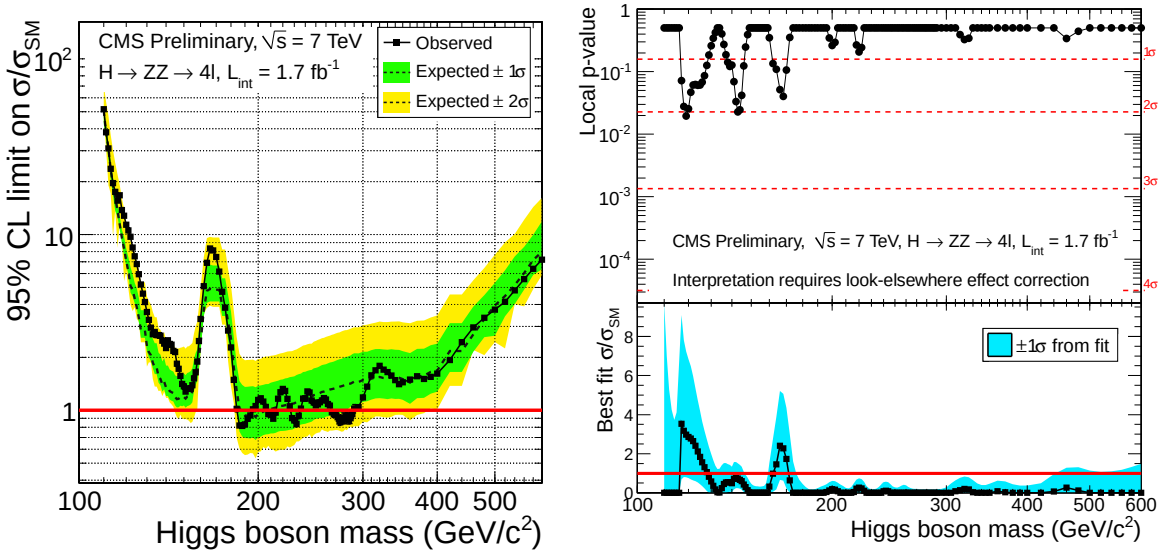

(a) (b)

Figure 16: $H \to ZZ \to 4\ell$ analysis: (a) Limits on the signal strength modifier $\mu = \sigma/\sigma_{SM}$ vs. hypothesized Higgs boson mass m_H. (b) Local p-value (top panel) and best-fit signal strength $\hat{\mu}$ (bottom panel) vs. hypothesized Higgs boson mass m_H.

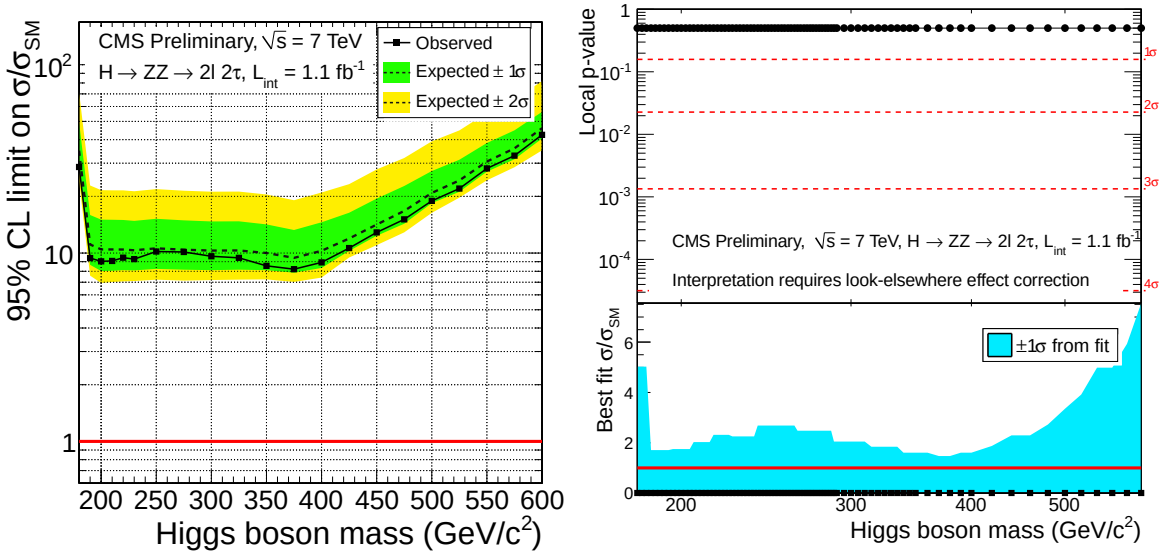

(a) (b)

Figure 17: $H \to 2\ell 2\tau$ analysis: (a) Limits on the signal strength modifier $\mu = \sigma/\sigma_{SM}$ vs. hypothesized Higgs boson mass m_H. (b) Local p-value (top panel) and best-fit signal strength $\hat{\mu}$ (bottom panel) vs. hypothesized Higgs boson mass m_H.

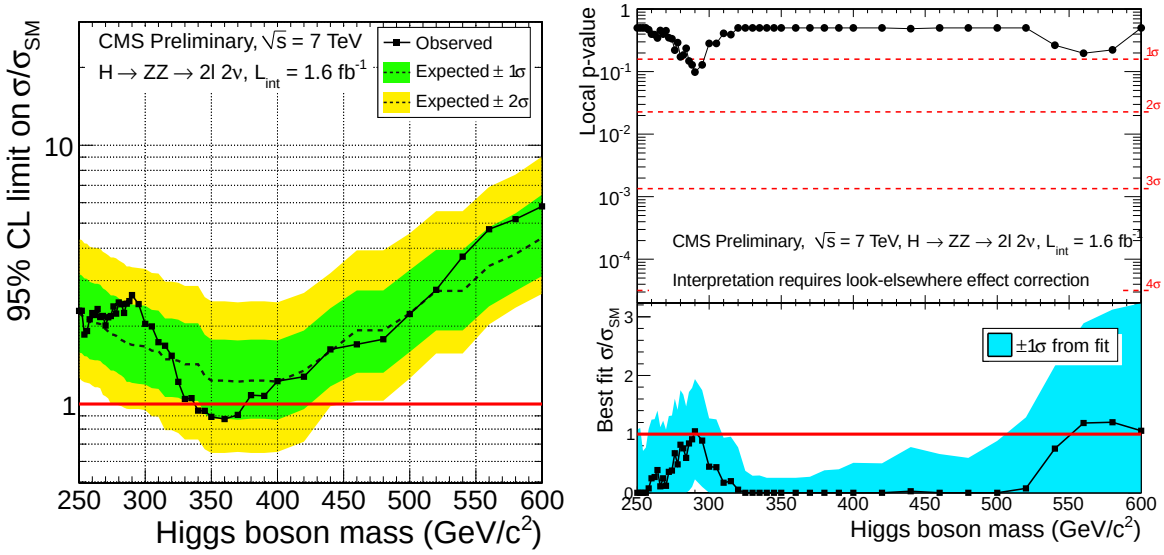

(a) (b)

Figure 18: $H \to 2\ell 2\nu$ analysis: (a) Limits on the signal strength modifier $\mu = \sigma/\sigma_{SM}$ vs. hypothesized Higgs boson mass m_H. (b) Local p-value (top panel) and best-fit signal strength $\hat{\mu}$ (bottom panel) vs. hypothesized Higgs boson mass m_H.

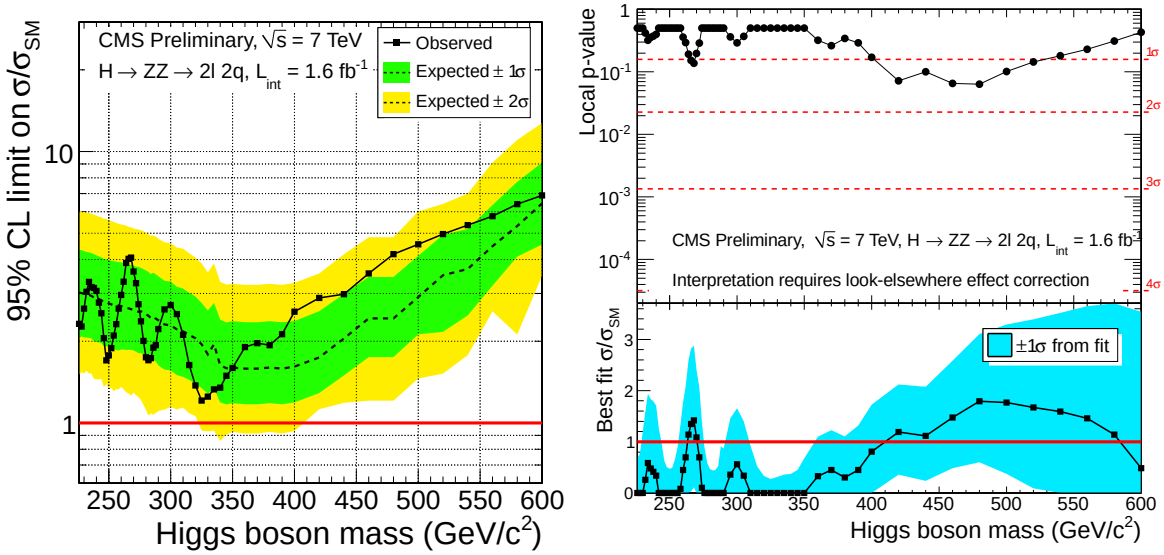

(a) (b)

Figure 19: $H \to 2\ell 2q$ analysis: (a) Limits on the signal strength modifier $\mu = \sigma/\sigma_{SM}$ vs. hypothesized Higgs boson mass m_H. (b) Local p-value (top panel) and best-fit signal strength $\hat{\mu}$ (bottom panel) vs. hypothesized Higgs boson mass m_H.

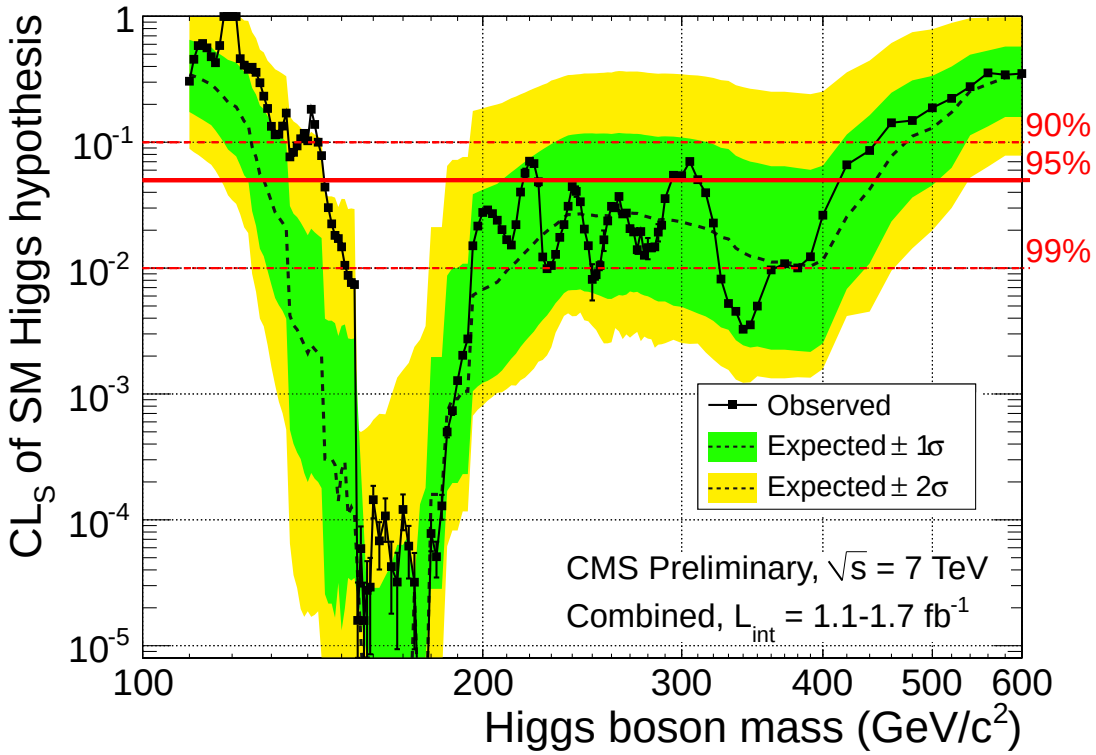

Figure 20: The CL_s value for the standard model Higgs hypothesis as a function of the Higgs boson mass in the range 110-600 GeV/c^2. The observed values are shown by a solid line. The dashed black line indicates the median expected CL_s value for the background-only hypothesis, while the green/yellow bands indicate the ranges that are expected to contain 68%/95% of all observed limit excursions from the median. The three red horizontal lines show confidence levels of 90%, 95%, and 99% defined as $(1 - CL_s)$.

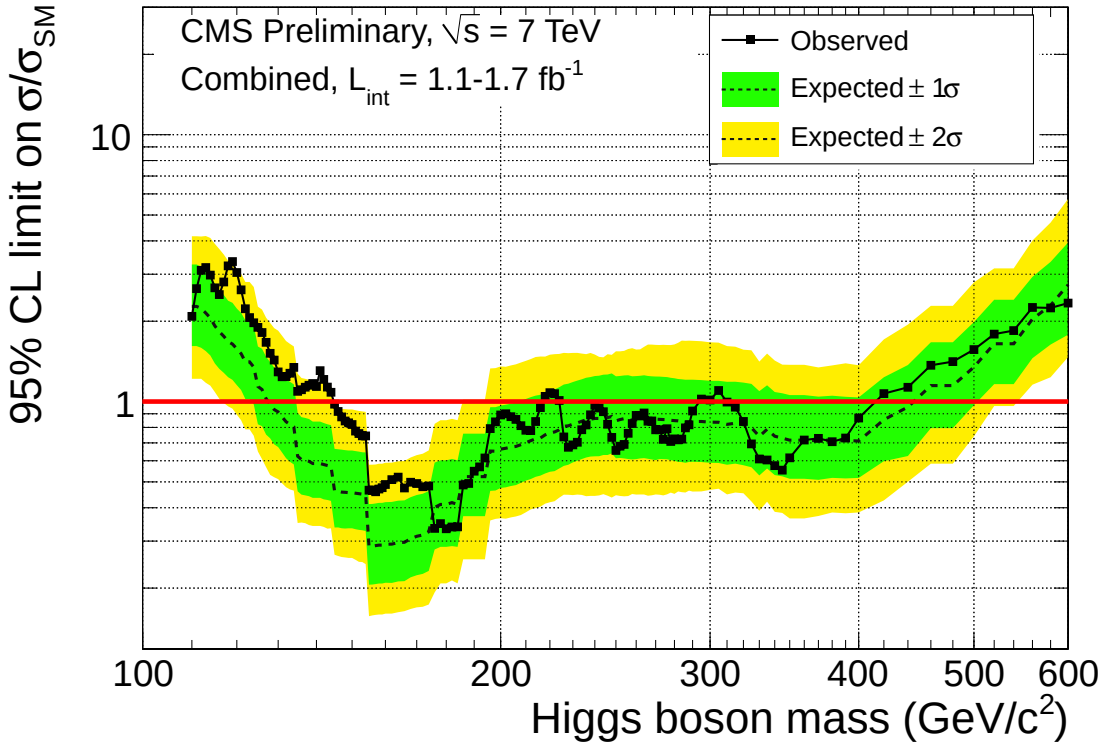

Figure 21: The combined 95% C.L. upper limits on the signal strength modifier $\mu = \sigma/\sigma_{SM}$, as a function of the SM Higgs boson mass in the range 110-600 GeV/c^2. The observed limits are shown by the solid symbols and the black line. The dashed line indicates the median expected limit on μ for the background-only hypothesis, while the green/yellow bands indicate the ranges that are expected to contain 68%/95% of all observed limit excursions from the median.

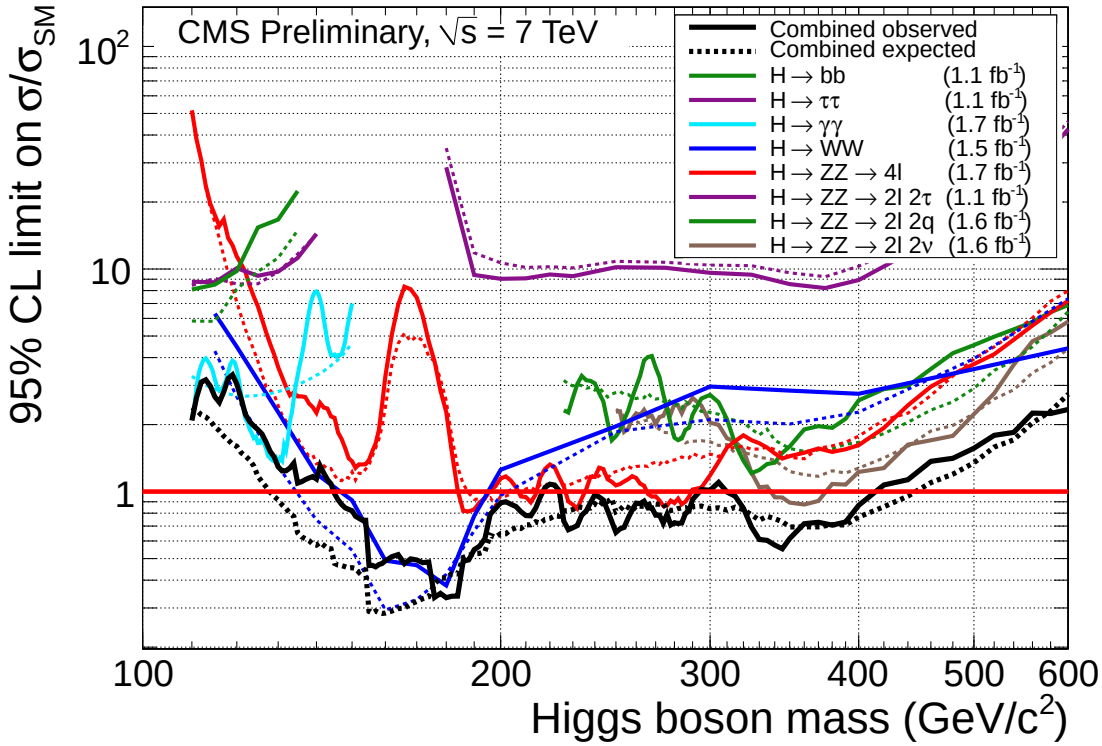

Figure 22: The observed 95% C.L. upper limits on the signal strength modifier $\mu = \sigma/\sigma_{SM}$ as a function of the SM Higgs boson mass in the range 110-600 GeV/c^2 for the eight major analyses and their combination. The limits are obtained with the CL_s method. The solid lines show the observed limits, while the dashed lines indicate the median expected assuming the *background-only* hypothesis.

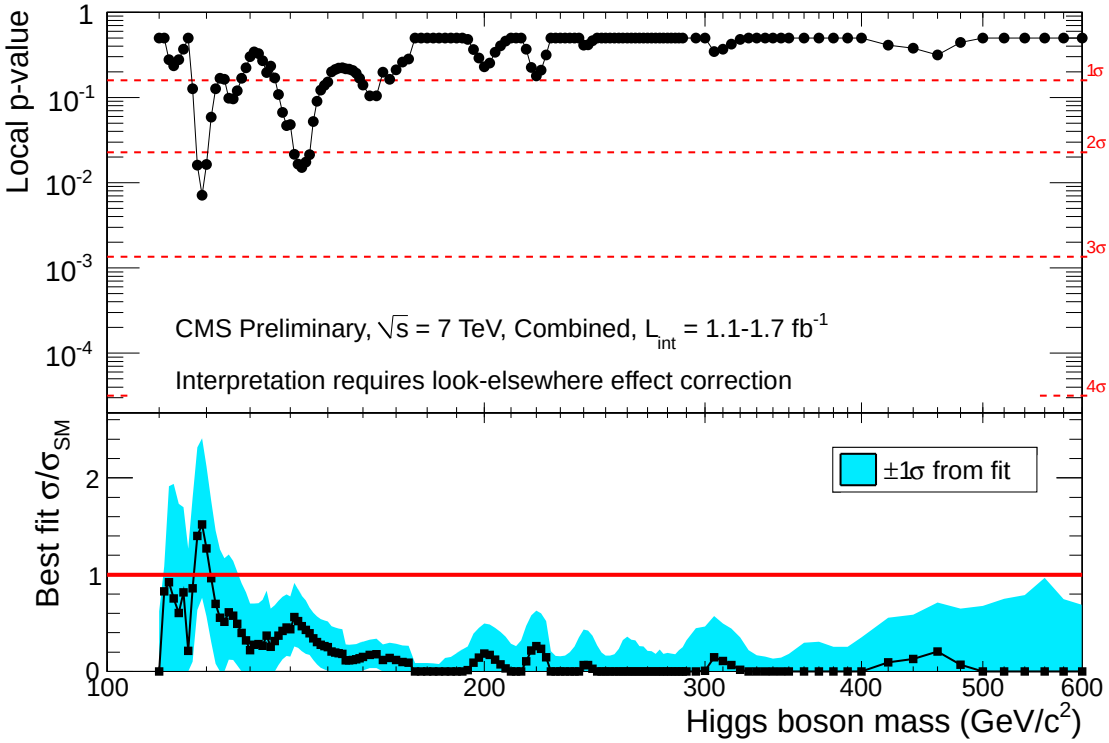

Figure 23: The *local* p-values (top) and observed best-fit signal strength $\hat{\mu} = \sigma/\sigma_{SM}$ (bottom) vs Higgs boson mass. The p-value is an estimated probability of upward background fluctuations as high or higher than the excesses observed in data. After taking into account the look-elsewhere effect (see text), the probability to see an excess at least as large as the one observed in data is ~ 0.4. The $\hat{\mu}$ value indicates by what factor the SM Higgs cross section would have to be rescaled to best match the observed data.

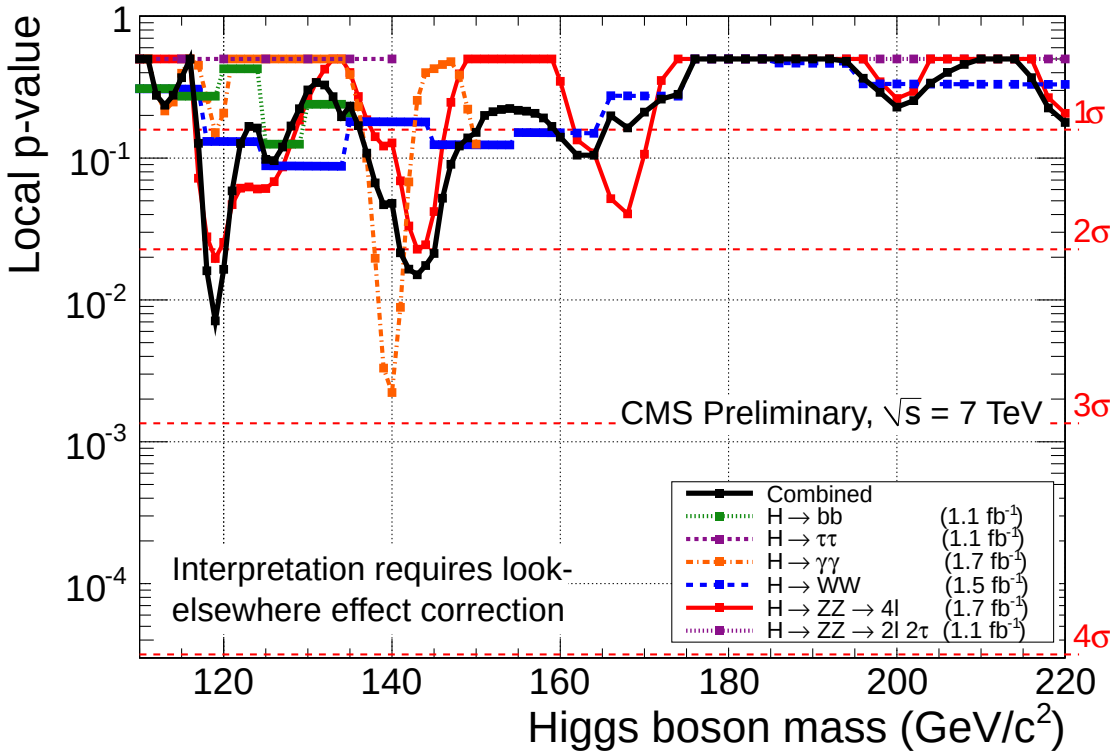

Figure 24: The overall combined *local* p-values (solid black line) and contributions of individual channels entering the combination vs. Higgs boson mass. The p-value is an estimated probability of upward background fluctuation as high or higher than the excesses observed in data. After taking into account the look-elsewhere effect (see text), the probability to see an excess at least as large as the one observed in data is ~ 0.4.

5 Conclusions

The CMS Collaboration has searched for the SM Higgs boson in pp collisions at a center-of-mass energy of 7 TeV in eight distinct Higgs decay final states: $H \to \gamma\gamma$, $H \to \tau\tau$, $H \to bb$, $H \to WW \to 2\ell 2\nu$, $H \to ZZ \to 4\ell$, $H \to ZZ \to 2\ell 2\tau$, $H \to ZZ \to 2\ell 2\nu$, and $H \to ZZ \to 2\ell 2q$. The amount of data used in these searches corresponds to 1.1-1.7 fb^{-1} of integrated luminosity. The Higgs boson mass range covered by these analyses spans from 110 to 600 GeV/c^2. To increase the overall experimental sensitivity to the presence of the signal, the search results obtained in these eight analyses have been further combined. The SM Higgs boson is excluded at 95% C.L. in three mass ranges 145-216, 226-288, and 310-400 GeV/c^2. The expected exclusion in the absence of a signal is 130-440 GeV/c^2. The largest excursion of the observed data from the expected has a probability of 0.4 after taking into account the look-elsewhere effect. At 90% C.L., we exclude the SM Higgs boson in the continuous mass range from 144-440 GeV/c^2. The reported limits were obtained using the modified frequentist construction known as the CL_s method.

Aknowledgments

We would like to acknowledge the very fruitful and collaborative effort of the LHC Higgs Combination Group, to which some of us formally belong.

References

[1] F. Englert and R. Brout, "Broken symmetry and the mass of gauge vector mesons", *Phys. Rev. Lett.* **13** (1964) 321–323. doi:10.1103/PhysRevLett.13.321.

[2] P. Higgs, "Broken symmetries, massless particles and gauge fields", *Phys. Lett.* **12** (1964) 132–133. doi:10.1016/0031-9163(64)91136-9.

[3] P. Higgs, "Broken symmetries and the masses of gauge bosons", *Phys. Rev. Lett.* **13** (1964) 508–509. doi:10.1103/PhysRevLett.13.508.

[4] G. Guralnik, C. Hagen, and T. Kibble, "Global conservation laws and massless particles", *Phys. Rev. Lett.* **13** (1964) 585–587. doi:10.1103/PhysRevLett.13.585.

[5] P. Higgs, "Spontaneous symmetry breakdown without massless bosons", *Phys. Rev.* **145** (1966) 1156–1163. doi:10.1103/PhysRev.145.1156.

[6] T. Kibble, "Symmetry breaking in non-Abelian gauge theories", *Phys. Rev.* **155** (1967) 1554–1561. doi:10.1103/PhysRev.155.1554.

[7] R. Barate and others (LEP Working Group for Higgs boson searches and ALEPH, DELPHI, L3, and OPAL Collaborations), "Search for the standard model Higgs boson at LEP", *Phys. Lett.* **B565** (2003) 61–75, arXiv:hep-ex/0306033. doi:10.1016/S0370-2693(03)00614-2.

[8] CDF and D0 Collaborations, "Combined CDF and D0 upper limits on Standard Model Higgs Boson production", (July, 2011). arXiv:1107.5518. CDF Note 10606 and D0 Note 6226.

[9] The ALEPH, CDF, D0, DELPHI, L3, OPAL, SLD Collaborations, the LEP Electroweak Working Group, the Tevatron Electroweak Working Group,and the SLD electroweak and

heavy flavour groups, "Precision Electroweak Measurements and Constraints on the Standard Model", *CERN-PH-EP-2010-095, http://lepewwg.web.cern.ch/LEPEWWG/plots/summer2010/, http://arxiv.org/abs/1012.2367* (2010).

[10] CMS Collaboration, "The CMS experiment at the CERN LHC", *JINST* **3** (2008) S08004. doi:10.1088/1748-0221/3/08/S08004.

[11] CMS Collaboration, "Search for a Higgs boson decaying into two photons in the CMS detector", *CMS PAS* **HIG-11-021** (2011).

[12] CMS Collaboration, "Search for Neutral Higgs Bosons Decaying to Tau Pairs in pp Collisions at $\sqrt{s} = 7$ TeV", *CMS PAS* **HIG-11-009** (2011).

[13] CMS Collaboration, "Search for the Standard Model Higgs Boson decaying to Bottom Quarks and Produced in Association with a W or a Z Boson", *CMS PAS* **HIG-11-012** (2011).

[14] CMS Collaboration, "Search for the Higgs Boson Decaying to W^+W^- in the Fully Leptonic Final State", *CMS PAS* **HIG-11-014** (2011).

[15] CMS Collaboration, "Search for a Standard Model Higgs boson in the decay channel $H \to ZZ^{(*)} \to 4\ell$", *CMS PAS* **HIG-11-015** (2011).

[16] CMS Collaboration, "Search for a Standard Model Higgs boson produced in the decay channel $H \to ZZ \to 2\ell 2\tau$ with CMS detector at $\sqrt{s} = 7$ TeV", *CMS PAS* **HIG-11-013** (2011).

[17] CMS Collaboration, "Search for the Higgs boson in the $H \to ZZ \to 2\ell 2\nu$ channel in pp collisions at $\sqrt{s} = 7$ TeV", *CMS PAS* **HIG-11-016** (2011).

[18] CMS Collaboration, "Search for the standard model Higgs Boson in the decay channel $H \to ZZ \to \ell^-\ell^+ q\bar{q}$ at CMS", *CMS PAS* **HIG-11-017** (2011).

[19] LHC Higgs Cross Section Working Group, S. Dittmaier, C. Mariotti et al., "Handbook of LHC Higgs Cross Sections: 1. Inclusive Observables", *CERN-2011-002* (CERN, Geneva, 2011) arXiv:1101.0593.

[20] ATLAS Collaboration, CMS Collaboration, and LHC Higgs Combination Group, "Procedure for the LHC Higgs boson search combination in summer 2011", *ATL-PHYS-PUB-2011-818, CMS NOTE-2011/005* (August, 2011).

[21] T. Junk, "Confidence level computation for combining searches with small statistics", *Nucl.Instrum.Meth.* **A434** (1999) 435–443, arXiv:hep-ex/9902006. doi:10.1016/S0168-9002(99)00498-2.

[22] A. L. Read, "Modified frequentist analysis of search results (the CLs method)", *CERN Yellow Report* **CERN-2000-005** (2000) 81.

[23] A. L. Read, "Presentation of search results: the CLs technique", *J. Phys. G: Nucl. Part. Phys.* **28** (2002) 2693.

[24] W. Fisher, "Systematics and Limit Calculations", (2006). Report No. FERMILAB-TM-2386-E.

[25] W. Fisher, "Collie: A Confidence Level Limit Evaluator", (June, 2009). D0 note 5595.

[26] T. Junk, "Sensitivity, Exclusion and Discovery with Small Signals, Large Backgrounds, and Large Systematic Uncertainties", (October, 2007). CDF/DOC/STATISTICS/PUBLIC/8128.

[27] G. Cowan, K. Cranmer, E. Gross and O. Vitells, "Asymptotic formulae for likelihood-based tests of new physics", *Eur. Phys. J.* **C71** (2011) 1–19.

[28] E. Gross and O. Vitells, "Trial factors for the look elsewhere effect in high energy physics", *The European Physical Journal C - Particles and Fields* **70** (2010) 525–530.

[29] L. Moneta, K. Belasco, K. Cranmer et al., "The RooStats Project", in *13th International Workshop on Advanced Computing and Analysis Techniques in Physics Research (ACAT2010)*. SISSA, 2010. arXiv:1009.1003. PoS(ACAT2010)057.

[30] Chen, M. and Korytov, A., "Limits and Signifcance". https://mschen.web.cern.ch/mschen/LandS/.

[31] S. Alioli, P. Nason, C. Oleari and E. Re, "A general framework for implementing NLO calculations in shower Monte Carlo programs: the POWHEG BOX", *JHEP*.

[32] T. Sjöstrand et al., "PYTHIA", *Comput. Phys. Commun.* **135** (2001) 238.

[33] D. d. F. G. Bozzi, S. Catani and M. Grazzini *Phys. Lett.* **B** (2003), no. 564, 65.

[34] S. Bernstein, "Démonstration du théorème de Weierstrass fondée sur le calcul des probabilités", *Comm. Soc. Math. Kharkov* **13** (1912) 1.

[35] CMS Collaboration, "Algorithms for b jet identification in CMS", *CMS Physics Analysis Summary* **CMS-PAS-BTV-09-001** (2009).

[36] J. Campbell and R. K. Ellis *Nucl. Phys. Proc. Suppl.* **205-206** (2010) 10–15. MCFM code: http://mcfm.fnal.gov/.

[37] CMS Collaboration, "Search for standard model Higgs boson in pp collisions at $\sqrt{s} = 7$ TeV", (July, 2011). CMS HIG-11-011.

[38] ATLAS Collaboration, "Combined Standard Model Higgs Boson Searches in pp Collisions at $\sqrt{s} = 7$ TeV with the ATLAS Experiment at the LHC", (July, 2011). ATLAS-CONF-2011-112.